January 2021

Reliability Analysis Of Low-Frequency Ac Transmission System Topology Of Offshore Wind Power Plants

Ashoke Kumar Biswas

RELIABILITY ANALYSIS OF LOW-FREQUENCY AC TRANSMISSION SYSTEM TOPOLOGY OF OFFSHORE WIND POWER PLANTS.

by

Ashoke Kumar Biswas

Bachelor of Science in Electrical and Electronic Engineering,

Bangladesh University of Engineering and Technology, Bangladesh, 1998

A Thesis

Submitted to the Graduate Faculty

of the

University of North Dakota

in partial fulfillment of the requirements

for the degree of

Master of Science in Electrical Engineering

Grand Forks, North Dakota

August

2021

Name: Ashoke Kumar Biswas

Degree: Master of Science

This document, submitted in partial fulfillment of the requirements for the degree from the University of North Dakota, has been read by the Faculty Advisory Committee under whom the work has been done and is hereby approved.

DocuSigned by:
Dr. Hossein Salehfar
6A3DA259C08E45F...
Hossein Salehfar, Ph.D., Chairperson

DocuSigned by:
Dr. Michael Mann
46FD545EE5FF405...
Michael Mann, Ph.D.

DocuSigned by:
Dr. Prakash Ranganathan
2E9D28B34204C6...
Prakash Ranganathan, Ph.D.

This document is being submitted by the appointed advisory committee as having met all the requirements of the School of Graduate Studies at the University of North Dakota and is hereby approved.

DocuSigned by:
Chris Nelson
2E0AE088C733403...
Chris Nelson
Dean of the School of Graduate Studies

7/1/2021
Date

PERMISSION

Title	Reliability Analysis of Low-Frequency AC Transmission System Topology of Offshore Wind Power Plants.
Department	Electrical Engineering
Degree	Master of Science

In presenting this thesis in partial fulfillment of the requirements for a graduate degree from the University of North Dakota, I agree that the library of this University shall make it freely available for inspection. I further agree that permission for extensive copying for scholarly purposes may be granted by the professor who supervised my thesis work or, in his absence, by the chairperson of the department or the dean of the School of Studies. It is understood that any copying or publication or other use of this thesis or part thereof for financial gain shall not be allowed without my written permission. It is also understood that due recognition shall be given to me and to the University of North Dakota in any scholarly use which may be made of any material in my thesis.

Ashoke Kumar Biswas
August 2021

TABLE OF CONTENTS

LIST OF FIGURES Page

LIST OF TABLES Page

ACKNOWLEDGMENTS

First and foremost, I would like to express my sincere and heartfelt gratitude to my advisor and mentor, Dr. Hossein Salehfar for his continuous guidance, support, and advice which he has provided me throughout the entire course of my research and study. His invaluable advice, guidance, enthusiasm, and motivation have pushed me to explore the breadth of my capabilities, and I will forever be indebted to him for this. I'm very fortunate to have him as my advisor.

I would like to extend my gratitude to my committee members, Dr. Michael Mann and Dr. Prakash Ranganathan for their acceptance of being on my committee as well as their constant support and guidance. I would also like to acknowledge the role of the School of Electrical Engineering and Computer Science at University of North Dakota (UND), Grand Forks, North Dakota for providing me the opportunity to study and conduct research.

My heartfelt thanks also goes to my friends, colleagues, and faculties for their unfailing support and encouragement throughout the years.

Above all, I am grateful to the Almighty God for giving me the opportunity and the chance to finish my thesis.

DEDICATION

To my parents

Kali Pada Biswas and Taramoni Biswas

and my wife

Ankhi Baidya

And my daughter

Ahona Arundhati

ABBREVIATIONS

DOE	Department of Energy
HVAC	High Voltave Alternating Current
HVDC	High Voltage Direct Current
LFAC	Low Frequency Alternating Current
FTA	Fault Tree Analysis
CIM	Critical Importance Measure
RRW	Risk Reduction Worth
AC	Alternating Current
DC	Direct Current
FFTS	Fractional Frequency Transmission System
XLPE	Cross-linked Polyethylene
kV	Killo Volt
OWPP	Offshore Wind Power Plant
VSC-HVDC	Voltage Source Converter-High Voltage Dirrect Current
MVA	Megga Volt Ampere
IGBT	Insulated Gate Bipolar Transistor
NPC	Neutral Point Clamp
PWM	Pulsed Width Modulated
MMC	Modular Multilevel Converter
SM	Sub Module

MW	Megga Watt
SCIG	Squirrel Case Induction Motor
kM	Killometer
DFIG	Dual Feed Induction Motor
PMSG	Permanent Magnet Synchronous Generator
AC/DC	Alternating Current to Direct Current
DC/AC	Direct Current to Alternating Current
SCR	Silicon Controlled Rectifier
ABB	Asea Brown Boveri
MIL-STD	Military Standard
XOR-gate	EXCLUSIVE OR-gate
MCS	Minimal Cut Set
BICS	Boolean Indicated Cut Sets
CCF	Common Cause Failure
MTTR	Mean Time to Repair
MTBF	Mean Time Between Failure
MIM	Marginal Importance Measure
DIM	Diagnostic Importance Measure
RAW	Risk Achievement Worth
WT	Wind Turbine
ST	Small Transformer
SSW	Small Switch

CT	Current Transformer
PT	Potential Transformer
IFAC	In Farm Alternating Current
XNOR	Exclusive NOR
LSW	Large Switch
LT	Large Transformer
IFDC	In Farm Direct Current
FMEA	Failure Mode and Effect Analysis
ARIMA	Auto Regressive Integrated Moving Average
RF	Random Forest
BCART	Bagging Classification and Regression Trees
SARIMA	Seasonal ARIMA
NREL	National Renewable Energy Laboratory
NMAE	Normalized Mean Absolute Error
NRMSE	Normalized Root Mean Squire Error

ABSTRACT

Many countries and regions of the world are planning to reduce the energy sector's carbon footprint and increase sustainable energy sources. To this end, wind power has become one of their primary renewable energy sources. However, wind power's significant challenges relate to the need for long transmission lines that connect the offshore wind power plants to the onshore grid. The three major transmission configurations and design topologies of High Voltage AC (HVAC) Transmission, High Voltage DC (HVDC) Transmission, and Low-Frequency AC (LFAC) Transmission for offshore wind power resources have been thoroughly discussed both in industry and academia. HVAC is the standard transmission system for short and long distances. In contrast, HVDC is a popular solution for the long-distance transmission of offshore wind power generators. In recent years, LFAC transmission topology at 20Hz has become an alternative solution to HVAC and HVDC transmission systems. The significant advantages of LFAC transmission are the substantial increment of transmissible power over traditional AC transmission systems and the elimination of offshore converter stations. The absence of an offshore converter system renders LFAC transmission less costly compare to the HVDC system.

The efficient design and reliability of offshore wind power transmission topologies are essential requirements for the transmission grid's smooth operation. This thesis work extensively investigated and reviewed the LFAC transmission topologies over HVAC and HVDC transmissions topologies of offshore wind power plans. Different methods are used to

assess the reliability performance of system designs. In this research, the state of the art of the simulation models for three transmission systems have been developed for reliability analysis of the above three transmission systems topologies using Fault tree analysis (FTA). This research has identified several reliability performance characteristics including minimal cut sets, importance measures, and time-based matrics (i.e, number of failures and mean unavailability) of the transmission systems, and compared these characteristics among three transmission systems. For reliability performance analysis, the time-base metrics, such as mean-unavailability and number of failures of the systems over 10,000 hours of operation, importance measures, or reliability importance measures, such as Critical Importance Measure (CIM) and Risk Reduction Worth (RRW), and Cut Sets have been calculated. The thesis has successfully identied major fault events for all the three transmission systems, and that the large switch is the most critical piece of equipment in the HVAC system, while the AC/DC or DC/AC converter is the most critical piece of equipment in the HVDC system, and the DC/AC converter and Cycloconverter are the most critical components in the LFAC transmission system. Furthermore, to enhance the offshore transmission systems reliability and ensure their smooth operation, effective and reliable offshore wind power generation predictions are critical. To this end, this research work also introduces the necessary offshore wind power forecasting tools.

1 INTRODUCTION

Wind energy has become a globally important dominant and sustainable energy source [1]. The energy challenges of the 21st century have created a need for clean energy solutions, a role that onshore and offshore wind energy resources can play in future solutions [2]. Environmental and economic concerns regarding the use of fossil fuels have highlighted the use of renewable energy sources as a substitute for existing fossil-fueled power plants [3]. Many countries have initiated steps to reduce carbon emissions by deploying more renewable energy sources, especially wind energy. The U.S. Federal Government has published new energy and environmental policies and objectives to expand renewable energy use significantly [4]. Experts predict global energy demand will rise 40% by 2040, and fossil fuels will offset two-thirds of the total demand [5]. A model has been developed by the U.S. Department of Energy (DOE), where 20% of U.S. electricity demand will be provided by wind energy by 2030 [6]. The potential of wind power makes it one of the key sustainable energy sources. However, several challenges, such as the shortage of land and public protests to large land-based wind farms, are driving offshore wind power plant developments.

As such, the feasibility studies and present research efforts are focusing on enhancing reliability and optimizing the investment of offshore wind farms. Generation, transmission, and integration projects of Offshore wind farms have started to become a good prospect of the wind energy industry around the world. This growth in offshore wind power projects ushers commercial and scientific challenges and opportunities for the design and construction of alternative economical transmission systems [7]. The offshore transmission of wind power

and its integration into the power grid has created many challenges, the mitigation of which are essential for sustainable energy supplies. There are three major transmission configurations and design topologies that have been thoroughly discussed both in the industry and academia. They are 1. HVAC Transmission, 2. HVDC Transmission, and 3. LFAC Transmission.

The efficient design and reliability of offshore wind power transmission topologies are essential requirements for the transmission grid's smooth operation. Different methods are used to assess the reliability performance of system designs. In this thesis, Fault Tree Analysis (FTA) has been used to analyze and compare the reliability performance of the above three transmission topologies. To further enhance the reliability performance of offshore wind power transmission systems, an efficient and effective wind power generation forecasting tool has been introduced. The output of the forecasting tool helps the transmission system operators to initiate proactive actions to bolster the transmission system's reliability.

1.1. Thesis Contribution

The advantages, disadvantages, and reliability performance features of LFAC transmission topology over those of HVAC and HVDC transmission topologies of offshore wind power plants are extensively investigated in the first part of this thesis. This thesis has also identified the efficiency and cost-effectiveness of the LFAC transmission system. In the second part of the research, the introduction of FTA into the power system industry has been extensively discussed, and the usefulness of the FTA method of reliability analysis of offshore wind power transmission systems has been identified. Using the FTA method, several offshore wind farm reliability performance measures, such as minimal cut sets, importance measure (i.e., Critical Importance Measure (CIM) and Risk Reduction Worth (RRW)), cut set

unavailability, component unavailability, system unavailability, minimal cut set occurrence rate, system occurrence rate, and the number of system failures have been computed and discussed.

In the third part of the research, state-of-the-art FTA simulation models of the three offshore wind power transmission systems have been built. The simulation models have successfully identified the minimal cut sets of each respective system, leading to the occurrence of the top respective failure event. The simulation models have also computed the minimum cut sets probability, component failure probability, and the system failure probability for all three transmission systems. The simulation models have also determined the time-based metrics such as the system mean unavailability and the number of system failures after 10,000 simulated hours of operation. The simulation models have also identified the CIM, and RRW of the system components.

The fourth part of the research has briefly evaluated and discussed the reliability performance characteristics of the LFAC compared to HVAC and HVDC transmission systems. The fifth part of this thesis has proposed a wind power generation forecasting tool to further increase offshore transmission system's reliability. As per the author's knowledge, to date, no such research on the reliability analysis of the LFAC transmission topologies of offshore wind power plants has been performed and presented.

1.2. Thesis Organization

Chapter 1 of this thesis first introduces the offshore transmission topologies and their reliability performance based on the FTA method. Next, a forecasting tool to enhance offshore wind power transmission system reliability is presented and discussed. Chapter 2 presents the literature review of the offshore transmission systems and their reliability analysis. Chapter 3

briefly discusses the economics of offshore transmission topologies and the cost-effectiveness of the LFAC system. Chapter 4 presents a short background on reliability and its applications. Chapter 5 presents the concepts of reliability analysis using the FTA method. Chapter 6 discusses the simulation models of offshore transmission systems. Chapter 7 presents and discusses the simulation results. Chapter 8 presents some forecasting methods to enhance the transmission system's reliability. Finally, Chapter 9 presents the conclusion and provides some direction for future work.

2. LITERATURE REVIEW

The simple configurations of three offshore transmission systems are shown in Fig. 1.

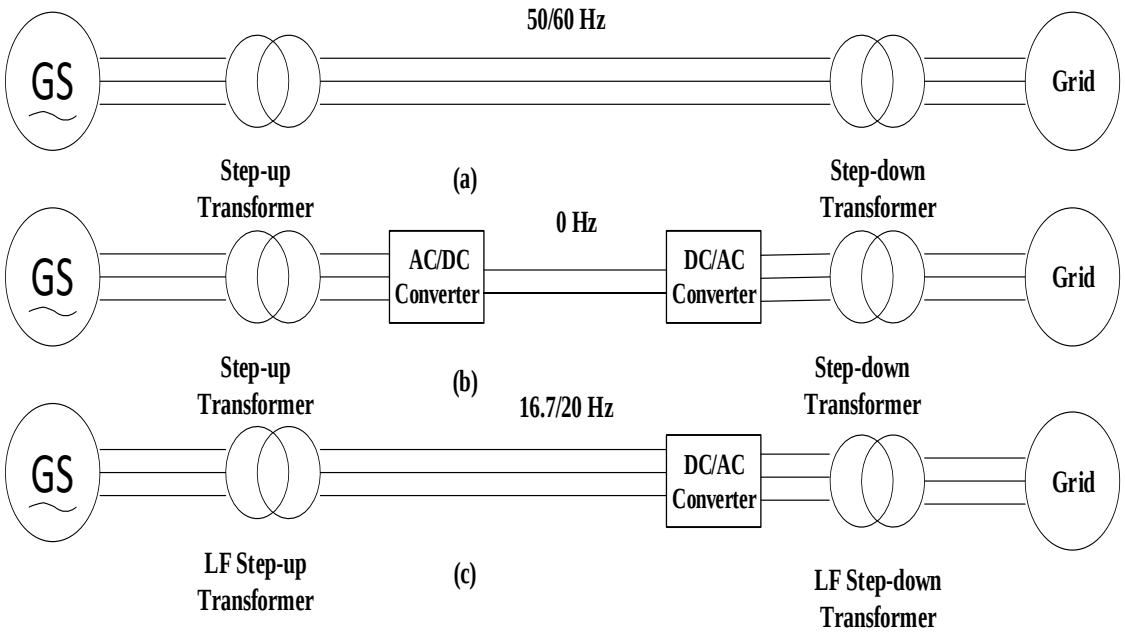

Fig. 1. Three simplified diagrams of transmission systems, (a) HVAC transmission system, (b) HVDC transmission system, and (c) LFAC transmission system [1].

The HVAC and HVDC transmission systems are used to transmit offshore wind power. HVAC transmission is usually used for small offshore distances as it is the most favorable up to 50 km from the shore [8], [9]. HVDC is the favored solution for long-distance offshore wind power transmission [7]. Due to the high charging current, HVAC cables cause heavy power losses, which makes HVAC transmission less suitable for long-distance energy transfer [10]. The advantage of HVDC transmission over HVAC transmission is that the transmission range can be much higher without any effect of reactive current and resonance in DC cables.

However, compared to HVAC, HVDC system is costly due to the power electronic converters. The theory of the fractional frequency transmission system (FFTS) was first proposed in 1994 [11]. In recent years, LFAC transmission topology has become prominent as a substitute solution to HVAC and HVDC transmission systems. The significant advantages of LFAC are the substantial increment of transmissible power over the traditional AC transmission systems and the exclusion of offshore converter stations. The absence of an offshore converter system renders LFAC transmission less costly compared to the HVDC system. However, the efficient operation of any offshore wind power generation system depends on the reliability of the transmission system. Thus, efficient techniques and methodologies for planning and obtaining the reliability and failure probability of the transmission system is critical [12].

Since the efficient and effective design and reliability of offshore wind power transmission topologies are paramount requirements for the offshore transmission grid's smooth operation, different methods are used to assess the reliability performance of system designs. In this thesis, the FTA method has been used for reliability performance analysis of the above three transmission systems topologies. The FTA concept was first implemented in Aerospace industries and then was accommodated by the nuclear power plant industry to qualify and quantify the hazards and risks involved in nuclear power plant production [13]. The FTA is gaining popularity in other industries because of its successful use in the nuclear power industry. The FTA method is a graphical representation technique that provides a substitute for reliability block diagrams. It is a top-down deductive analysis approach that starts from the top event selected by the user. The significance of FTA lies in its capability to identify the root cause and providing a visual model of how each piece of equipment can be

failed, considering both external and internal factors [13]. For production planning purposes, efficient and accurate offshore wind power generation predictions are essential. As a result, to enhance the transmission system's reliability performance, effective and reliable single-stage and hybrid forecasting models have been introduced and discussed.

3 TRANSMISSION TOPOLOGIES

3.1 HVAC Transmission

HVAC transmission system is one of the effective methods for offshore wind power transmission at 50 or 60 Hz, where the distance is less than 50 km to shore [7], [14]. Normally, wind farms which are near the shore are installed with HVAC transmission as considering the cost [7], [15]. A typical offshore wind farm integration and a simplified layout of an offshore HVAC transmission topology are shown in Fig. 2 [7] and Fig. 3 [2], respectively. To connect the offshore and onshore substations, as shown in this configuration, cross-linked polyethylene (XLPE) cables are usually used. Two offshore transformers have stepped up 33 or 66 kV voltage from the collector end to the transmission level voltage of 110, 150, or 220 kV. The parallel transformers are used to boost the export power availability, which is rated at 60% of the nominal power of the Offshore Wind Power Plant (OWPP) [16].

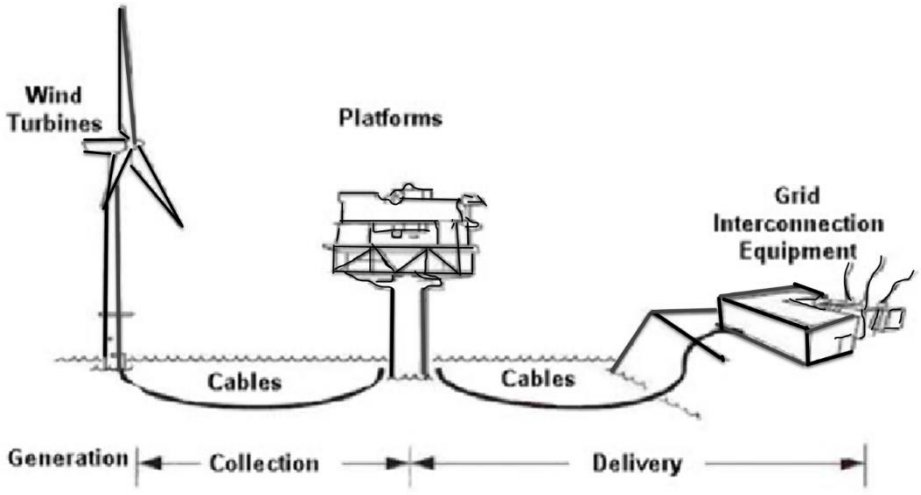

Fig. 2. A typical offshore wind farm integration [7].

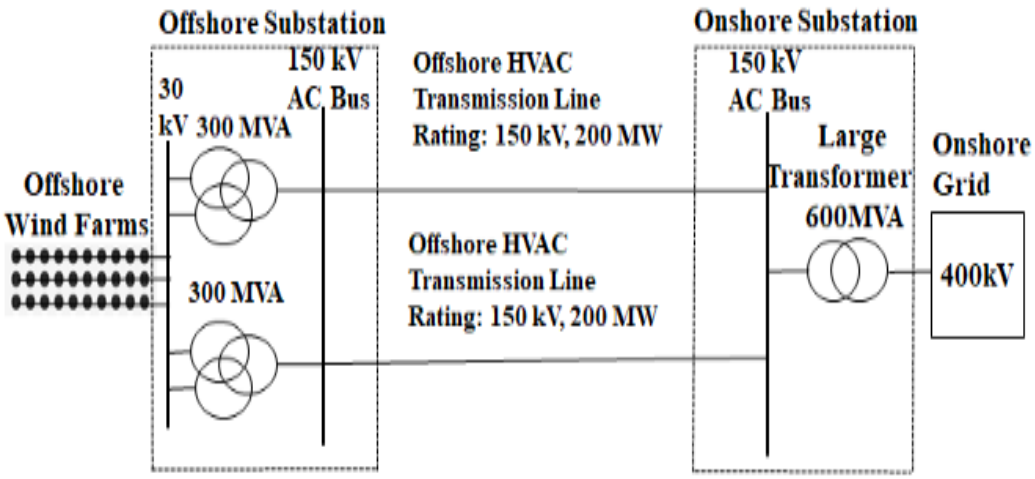

Fig. 3. A simplified layout of an offshore HVAC transmission topology [2]

The HVAC transmission system is technically impractical for long distance offshore sites due to the higher capacitance of the cables, which produces reactive current and causes high power losses. The amount of this reactive power is proportional to the distance and the square of the system voltage [17], [18].

3.2 HVDC Transmission

HVDC transmission system is the leading technology for offshore wind power transmission over 200 km, but the system is costlier [7]. The major components of HVDC transmission are the two converter stations and the undersea transmission cable connecting these converters. The converter in the offshore site works as a rectifier, and the onshore converter operates as an inverter at variable frequency, and both of them can consume or supply reactive power to the AC grid [2]. Considering the cost benefits, direct current (DC) cables are used for longer distances [19]. The major advantage of an HVDC transmission system is low transmission losses. The DC transmission power losses are approximately 3% per 1,000 km, and the power losses of the converter station are approximately 1.5% of the

nominal transmission power [20]. The basic configuration of an HVDC transmission topology is depicted in Fig. 4 [2].

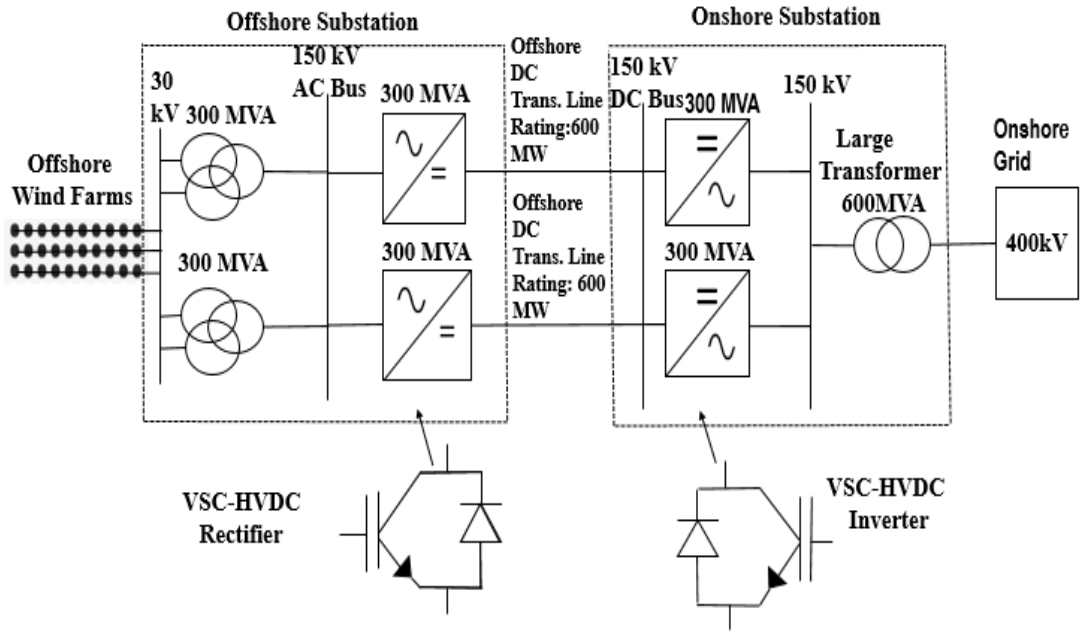

Fig. 4. Basic configuration of HVDC solution [2]

The two major transmission methodologies for the HVDC transmission of offshore wind power are as follows:

1. Thyristor based HVDC
2. Voltage source converter-HVDC (VSC-HVDC)

3.2.1 Thyristor based HVDC

Thyristor-based DC conversion has been widely used for electric power conversion, where the principle of line commutated frequency conversion is applied to control current [18]. This conversion is a reliable technology for the transmission of bulk power up to several gigawatts. Figure 5 illustrates a thyristor-based HVDC converter [21], [22], [23], which comprises two six-pulse bridges on the DC side connected in series, and a phase shift used between the

respective AC power sources to eliminate harmonic voltages and currents. A converter transformer with two different secondary windings, or valve windings, is placed between the two AC sources to create a phase offset of 30 degrees [22], [23]. Thyristor-based rectifiers and inverters require reactive power for commutation, that can be delivered by a source tied with the power grid or a reactive power source similar to a large synchronous generator linked to the offshore grid [20]. The thyristor (12-pulse) HVDC technology is shown in Fig. 5 [20].

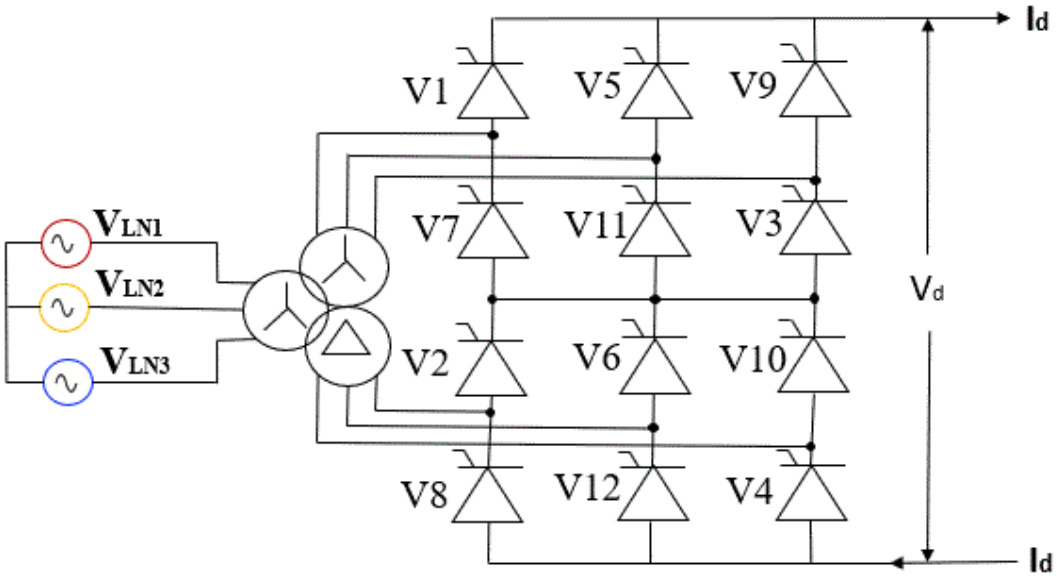

Fig. 5. Thyristor (12-Pulse)-HVDC Technology [20].

3.2.2 Voltage Source Converter-HVDC (VSC-HVDC)

VSC-HVDC transmission system was developed after the introduction of the Insulated Gate Bipolar Transistor (IGBT) as a power electronic device [17] used in offshore rectifier systems. The inverter at the onshore side connects the wind farm with the grid and works as an interface to supply the energy into the grid. This system's advantage over the conventional thyristor-based system is that it has an independent reactive power control at the onshore converter station, nearly completely free of fault currents and commutation failures [20]. The commercial HVDC VSC is marketed by Siemens commercially as HVDC light and HVDC

plus and was commissioned first by Asea Brown Boveri (ABB) in Hellsjön, Sweden, in 1997 [23].

3.2.2.1 Neutral Point Clamped (NPC) Converter

The VSC technology described above has been improving over time, and the three-level Pulse-Width-Modulated (PWM) controlled converters and Modular Multilevel Converters (MMC) have been developed to increase its efficiency. The neutral point clamped (NPC) converter is used broadly in the industry due to low harmonic generation and the reduction of losses to approximately 1.7% [24]. The NPC three-level converter of VSC-HVDC technology is illustrated in Fig. 6 [20], [25].

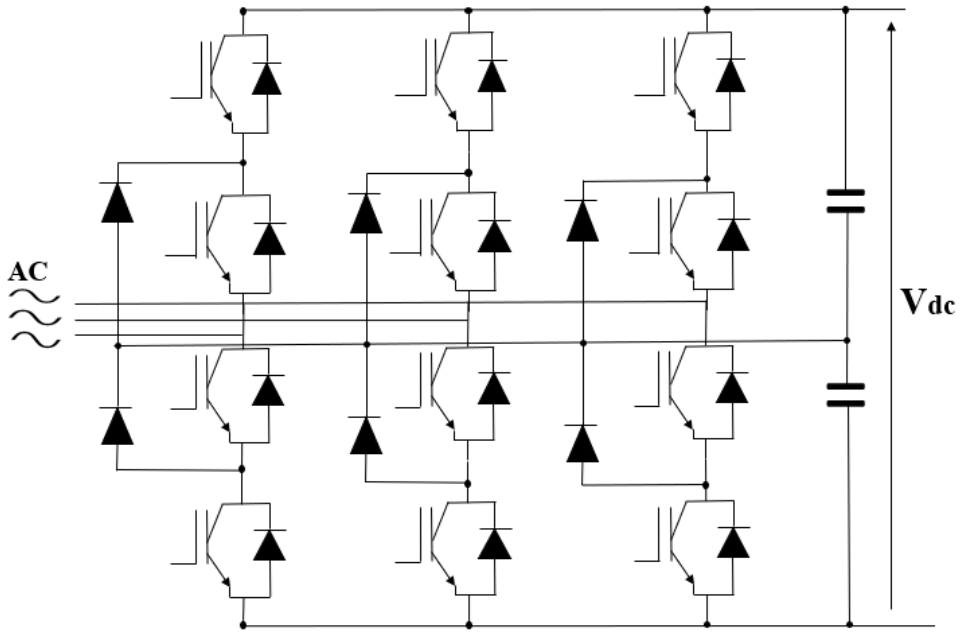

Fig. 6. VSC-HVDC Technology with NPC three-level Converter [20], [25].

3.2.2.2 Modular Multilevel Converter (MMC)

The MMC is currently developed by cascading multilevel converter based on a series of submodule connections. This converter generates a staircase voltage waveform, the shape of which depends on the number of submodules (SM). As the number of submodules is increased, the waveform becomes more sinusoidal [9], [25]. The VSC- HVDC technology with MMC is demonstrated in Fig. 7 [9], [25].

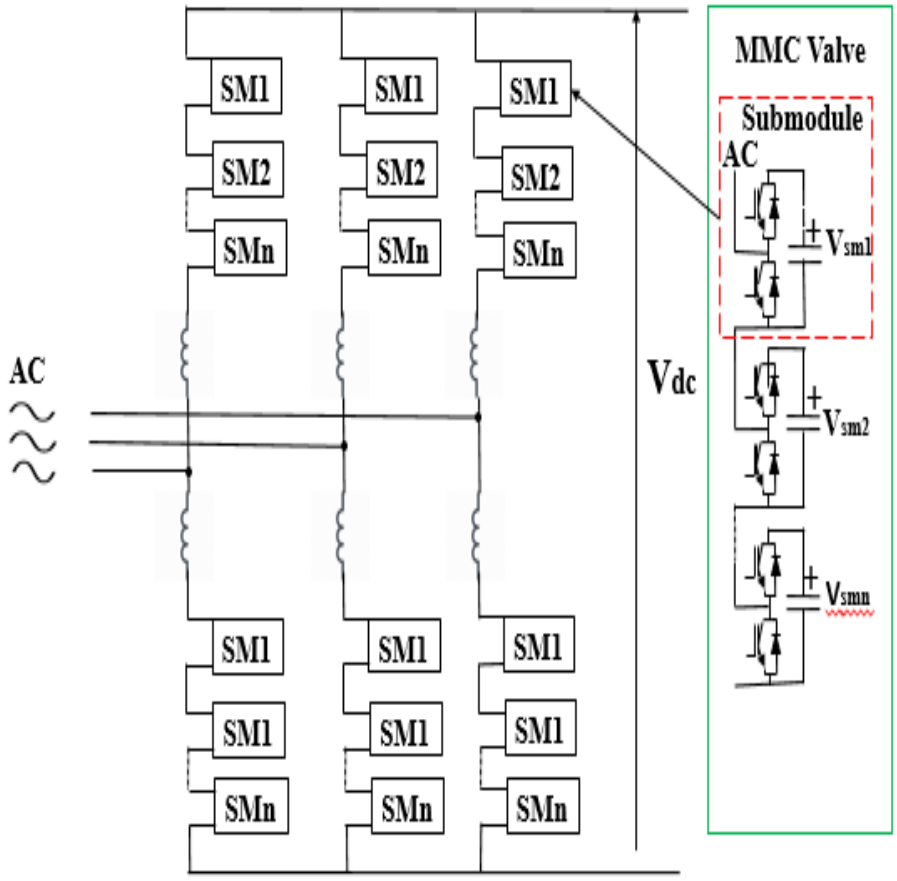

Fig. 7. VSC-HVDC technology with Modular Multilevel Converter (MMC) [9], [25].

3.3 LFAC Transmission

LFAC transmission system offers precise control and design advantages over conventional AC transmission. The transmission distance can be extended at a lower frequency and can eliminate the complexity of offshore converter stations with a reduced cost. The simplified network diagram of LFAC transmission system is shown in Fig. 8 [10].

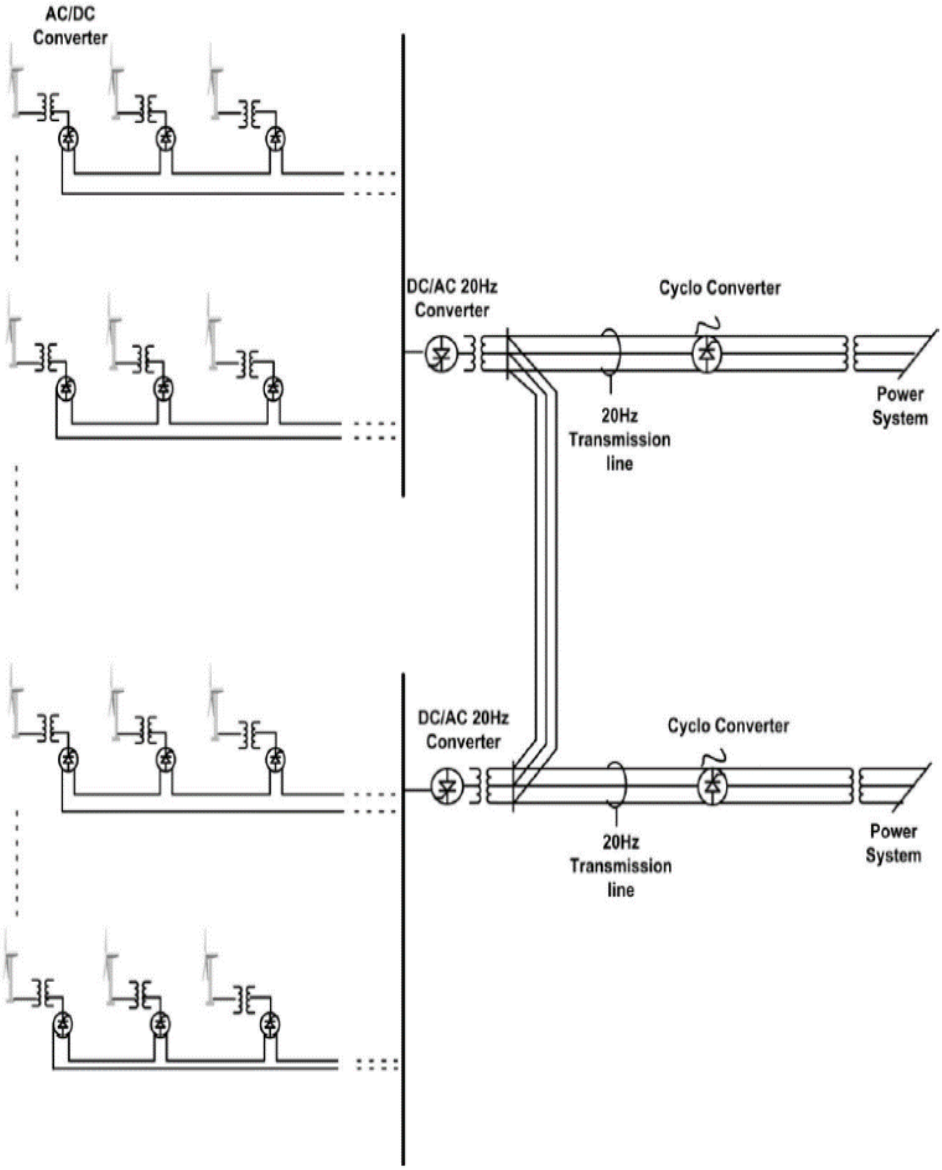

Fig. 8. Low-Frequency AC Transmission system [10]

LFAC is the derivative of HVAC transmission systems, and the working frequency is one-third of the 60 Hz nominal frequency. The advantage of low-frequency transmission is that it increases the power transfer capacity and transmission distance as compared to HVAC [7]. Another major benefit of LFAC is that no offshore converter station is required. The absence of an offshore converter in the system has enhanced reliability and minimizes complexity and cost [26]. The low-frequency system transmits power from the collector network at a lower 20 Hz frequency to Cycloconverter. Cycloconverter works as a frequency conversion device and converts the low frequency to 60 Hz grid frequency. The system becomes comparatively simpler than the HVDC system, as the number of conversion steps is lower.

3.3.1 The Background of LFAC Transmission

Countries such as Germany, Austria, Norway, Switzerland, and Sweden, mainly use the low frequency of 16.667 Hz at 15 kV, and Costa Rica and the USA use 20 Hz and 25 Hz, respectively, in the electric traction system [7], [27] . In the past, DC motors were used for electric traction due to their speed control characteristics. Since DC is not a viable option for long distance railway lines, universal motors for AC traction are proposed. Eddy currents induced by the winding of a universal motor can cause overheating at a nominal 60 Hz frequency. Low-frequency propulsion motor operation was proposed to alleviate overheating, reduce losses, and reduce design complexity [7], [28]. The low frequency system is suitable for long distance railways lines [7]. In 1994, X. Wang first proposed the Fractional Frequency AC Transmission System (FFTS) for transmission of hydroelectric power over long distances [11], [29].

3.3.2 Advantages of LFAC

A major benefit of the LFAC topology is to significantly reduce transmission system costs for remote or offshore wind farms compared to power frequency AC or HVDC transmission alternatives. This topology also offers numerous operational advantages, such as high reliability, better scheduling of wind resources, more efficient and centralized utilization of storage, and the ability to withstand voltage and reactive power fluctuations [10].

3.3.3 LFAC Basic Principle

The charging current or reactive current is the primary restraint for power transmission capability in the HVAC system. The charging current (I_c) relates to the frequency (f) as shown in eq. (1) [7].

$$I_c = 2\pi f l C E \tag{1}$$

The reactive power Q_c and the active power transmission P are shown in eq. (2) and (3), respectively.

$$Q_c = I_c E = 2\pi f l C E^2 \tag{2}$$

$$P = \sqrt{S^2 - (2\pi f l C E^2)} \tag{3}$$

where C = Cable capacitance,

S = Apparent power, MVA

P =Active Power of the Transmission line, MW, and

E = Nominal Voltage, kV.

The transmission capacity can be increased by reducing cable reactance. The impedance of the line mainly depends on the line reactance X_L and is directly proportional to frequency as shown in eq. (4).

$$X_L = 2\pi f L \tag{4}$$

Eq. (3) shows that the decrease in frequency can lead to an increase in the active power. Transmission capacity can be enhanced by reducing the transmission line reactance. So, low frequency is used in LFAC system to increase transmission capacity. For example, using 20 Hz, the transmission distance can be increased ideally three times the transmission distance at 60 Hz [7].

3.3.4. Offshore Wind Turbine Design

The design of wind turbines in LFAC transmission systems is one of the most important considerations. Decreasing the frequency increases the size of the transformer. In the current wind farm scenarios, the transformer and the converter are located in the nacelle of the turbine [7], [30]. As such, larger transformers at low frequency will need turbines with larger nacelles. The characteristics of LFAC also relate to the type of generator used. Liserre et al. have proposed alternative generator configurations for megawatt (MW) wind farms, such as Squirrel Cage Induction Generator (SCIG), Dual Fed Induction Generator (DFIG), and Permanent Magnet Synchronous Generator (PMSG) [7], [31]. In recent years, PMSG-based offshore wind farms have become more popular than other configurations due to their lower weight, constant speed, size and maintenance [7], [32], [33], [34]. PMSG combined with fully rated converters can generate low frequency power for LFAC systems.

3.3.5. Low frequency AC transformer

The major benefit of LFAC is the removal of converter station at offshore, which significantly reduces the requirements of offshore platform space, but it increases the size of offshore the transformer, and this is the fundamental obstacle to the LFAC transmission system. The voltage of the transformer is shown in eq. (5), indicating that the reduction in frequency would lead to an increase in either the width of the core or the number turns [7], [35].

$$E = 4.44fBNA \tag{5}$$

where E = Applied voltage,

f = Frequency,

B = Flux density,

N = Number of turns, and

A = Core cross-sectional area.

The thickness of the core may increase around 1.43 times of traditional 60Hz transformers [7], [35]. So, if we decrease the frequency three times, the cross-section area of the transformer will increase three times.

3.3.6 LFAC System Configuration and Control

A simplified diagram of LFAC system configuration and control is shown in Fig. 9 [10].

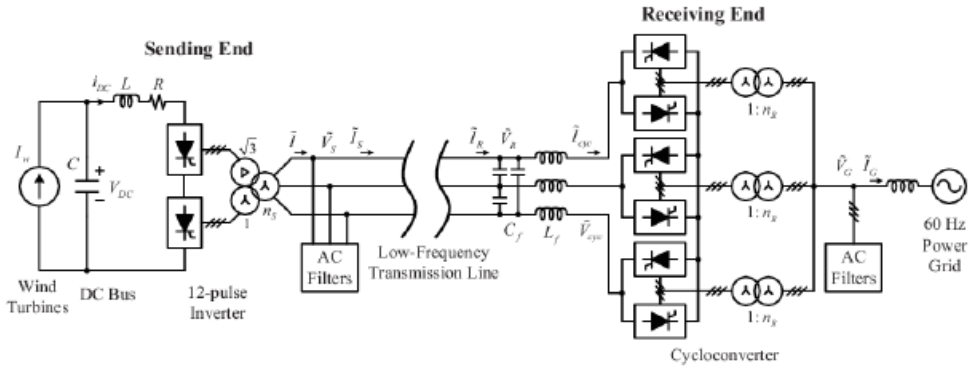

Fig. 9. The Simplified Diagram of LFAC Transmission System and Control [10]

In Fig. 9, the output of wind turbine has been rectified and connected to a collection of medium voltage dc bus. The rectifier output is represented as a dc current source I_w with a fixed voltage. A 12-pulse thyristor-based inverter has been used to convert the dc power to

low frequency ac power (20 Hz). The LFAC system uses the same standard transformer used in HVAC system. However, the ratings of transformer will be reduced accordingly, which means transformer of same ratings in LFAC transmission system will be bulky and heavier than the transformer in the conventional 60 Hz system. AC filters are utilized to remove current harmonics, as well as to deliver reactive power to the converter in the transmission line. For interfacing the low-frequency transmission line and the 60 Hz transmission grid, a three-phase bridge Cycloconverter with 36 thyristors is used, and odd current harmonics are suppressed by Grid side filters [10].

3.3.7 Cycloconverter

The term Cycloconverter is generally used to depict the ac-ac conversion process. In practice, frequency conversions are typically accomplished with a specialized form of nonlinear phase modulation, where rectifier like circuits performs this operation. A positive and negative converter together support ac-ac conversion. This system is normally referred to as the Cycloconverter. A simple Cycloconverter circuit is shown in Fig. 10.

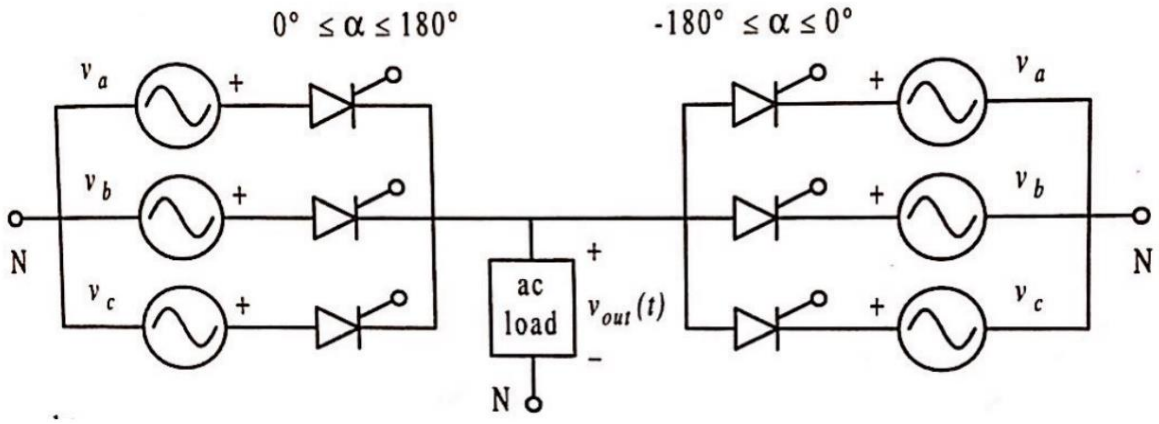

Fig. 10. A Cycloconverter: positive and negative converters combine to support ac-ac conversion with SCRs [36].

4 RELIABILITY AND ITS APPLICATIONS

4.1 The History of Reliability

The field of reliability engineering can be seen when humans started to rely on machines for a living. The ancient pump Noria is considered to be the world's first revolutionary machine which used hydraulic energy from the flow of a river or stream, and transferred water to troughs, viaducts and other distribution devices to irrigate fields and supply water to communities [37]. Reliability engineering really flourished with the progress of the commercial aviation industry after the World War II [38]. It became a paramount interest to the aviation industry management. Since aviation accidents are costly and high-profile in nature, the aviation industry deemed it necessary to seriously develop reliability engineering as a scientific discipline. In 1950, US Air Force formed an ad hoc group to investigate the reliability of the general equipment, and the Defense Department created the Advisory Group on Reliability of Electronic Equipment (AGREE) [38]. In 1970s, the reliability engineering focused on using the fault tree analysis (FTA) method for nuclear reactors safety [38]. Reliability engineering methodologies have also been used to maintain the effective operational fitness of military equipment in defense industry. Military Standard (MIL-STD) is largely involved in the reliability engineering field or many reliability engineering standards are originated from military activities.

4.2. The Concept of Reliability

The basic definition of reliability is the probability of a product successfully functioning as expected for a specific duration of time within a specified environment [38], [39]. With the efficient use of reliability engineering concepts and techniques, we can enhance systems performance, safety, increase output, and increase profitability. Incorporating

reliability at the early product design stages, safe and efficient designs along with optimal maintenance and availability plans of complex engineering systems can be developed.

Maintainability is the probability of reinstatement to normal operating mode from a failed mode of equipment, machine, or system within a specific time-frame [38], [39]. On the other hand, availability is a characteristic of a system to function as expected on demand. Availability is the percentage of time the system is functioning per year [38], [40].

The people who are involved in manufacturing and other industries incorporate reliability engineering techniques into their design deliberations and strategic objectives and actions. This includes most of the important areas such as machines and systems design, procurement, and plant operations and maintenance. Reliability engineering handles the sustainability and dependability of equipment, parts, and systems. It also integrates a large variety of demonstrative tools to identify the characteristics of the failure of the equipment and product. Normally, the ultimate goal of the reliability engineering field is focused on product reliability and dependability assurance [39].

4.3 Power System Reliability

A power system supplies electricity to the customers and tries to mitigate the demand at a certain degree of reliability and cost. Today the society expects our supply of electricity to be continuous and uninterrupted. To achieve this objective, power system managers and engineers utilize technical and financial investments during planning, operating, or both. The probabilistic assessment of power system behavior was first introduced in the 1930s [41]. The power-system reliability concept is a broad topic and its main focus to satisfy the consumer need for uninterrupted electricity [42]. Nowadays, all power system utilities have developed some form of reliability evaluation techniques, and the power system planners are focusing

their goals on maintaining system reliability for ensuring adequate electricity supplies [42]. Power system utilities, especially offshore power transmission utilities, can use the FTA tool to maintain reliable electricity production and supply to the grid, as well as the customers.

5 RELIABILITY EVALUATION USING FAULT TREE ANALYSIS

5.1 Background of Fault Tree Analysis

The concept of fault tree analysis (FTA) was first proposed by Bell Telephone Laboratories to execute a safety assessment of the Minuteman Launch Control system in 1961 [43]. The University of Washington and the Boeing Company sponsored a Safety Symposium in 1965 where several papers were presented on details of the FTA. The presented papers highlighted the utility of the FTA as a reliability tool in the nuclear reactor industry. Great success in reliability assessment of complex systems was reported in the first part of the 1970s [38], [43].

The Aerospace industry first implemented the concept of FTA, and then the nuclear power plant industry utilized FTA to analyze the hazards and risks associated with nuclear power generation [14]. FTA technique is also being popularized in other industries because of its effective utilization and application in the nuclear power industry. FTA graphically represents the Boolean logic associated with the design of specific system failure, or top event, and basic failure or the primary events [38], [44], [45], [46]. FTA is essentially a top-down deductive and graphical analysis technique, extensively used in reliability and safety measurement [38], [46], [47]. This technique can detect the various combinations of component failures and human error that could lead to a specified unwanted system failure [47], [48]. The top event is defined as the undesired output or the failure of the whole system. The FTA converts a physical system into a structured logic diagram in which certain events lead to one specified TOP event [47], [48]. Basic and intermediate events are the contributory events or the causes of the system's failure, connected to the top events through various gates forming the chain of events or failure combinations [47].

Gates and events are the primary building blocks of FTA. To integrate and connect different possible failure events, the logic Gates are used in the fault tree diagram. The purpose of the fault tree diagram is to show the underlying dependency of the top-level failure event to the next level of failures and determine the possible causes of failure. FTA utilizes a fixed failure rate of basic level events to identify the probable occurrence rate of the top event.

5.2 Symbology of FTA

A fault tree comprises a variety of symbols as discussed next.

5.2.1 Primary Events

The primary events of FTA are the events that are not further developed [38]. For the computation of the probability of a top event, the primary events probabilities have to be provided in the fault tree diagram. There are four types of primary events in FTA. They are illustrated as follows [38], [43], [49], [50], [51], [52], [53], [54], [55]:

5.2.1.1 Primary Events and Symbols

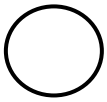

Basic Event: A basic event is represented by a circle and will not develop further.

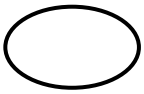

Conditioning Event: Specific conditions or restrictions that apply to any logic gate used normally with PRIORITY and INHIBIT gates.

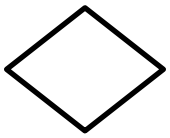

Undeveloped Event: An event which is not further developed due to insufficient consequence or information unavailability.

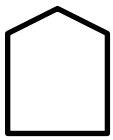

External Event: The house symbol is used to present an event which is normally expected to occur, for example: a phase change in a dynamic system.

5.2.2 Intermediate Events

Intermediate Event: A fault event that happens due to one or more antecedent failures.

5.2.3 Gate Symbols

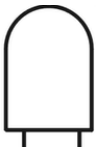

AND - Output fault takes place when all of the input faults happen.

OR - Output fault only materializes when at least one input fault generates.

EXCLUSIVE OR: If only one fault occurs in input, output fault occurs.

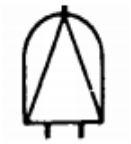

PRIORITY AND: Output fault exists when all of the input faults occur in a definite sequence.

INHIBIT - Output fault takes place when the single input fault occurs for the presence of an enabling condition.

5.2.4 Transfer Symbols

Transfer in – Illustrates that the tree is developed further for the presence of the corresponding Transfer out

Transfer out – Illustrates that this part of the tree must be linked to the corresponding Transfer in.

5.3 Gate operations

5.3.1 OR-gate Operation

Fig. 11 illustrates a two-input OR-gate where events A and B are input events, and Q is the output event. The output event Q takes place when event A occurs, or B occurs, or A and B happen simultaneously.

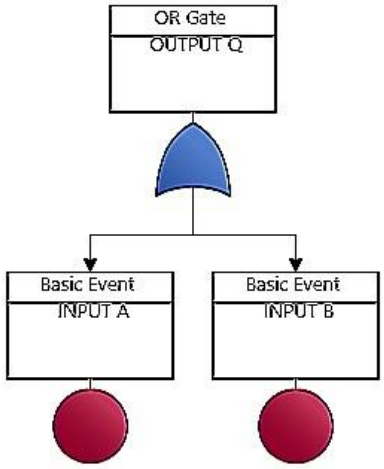

Fig. 11. Two input OR-gate

The Boolean output Q of the OR-gate is expressed as shown in eq. (6) [38], [50], [51], [53].

$$Q = A \cup B$$
$$= A + B \tag{6}$$

For n number of input events linked to the OR-gate, the equivalent Boolean expression [38], [50], [51], [53] is as follows:

$$Q = A_1 \cup A_2 \cup A_3 \cup \ldots\ldots \cup A_n$$
$$= A_1 + A_2 + A_3 + \cdots \ldots A_n \tag{7}$$

The probability of eq. (7) is defined as [38], [50], [51], [53], [54]:

$$P(Q) = P(A) + P(B) - P(A \cap B) \text{ or}$$
$$= P(A) + P(B) - P(A)P(B|A) \tag{8}$$

If A and B are mutually exclusive events, then

$$P(A \cap B) = 0, \text{ and}$$

$$P(Q) = P(A) + P(B) \tag{9}$$

If A and B are independent events, then [39]

$$P(B|A) = P(B) \text{ and}$$

$$\mathrm{P(Q) = P(A) + P(B) - P(A)\ P(B)} \tag{10}$$

If event B solely depends on event A, then

$$P(B|A) = 1, \text{and}$$

$$P(Q) = P(A) + P(B) - P(A) = P(B) \tag{11}$$

5.3.2 AND-gate Operation

The And-gate is used to display the output when all the inputs occur. Fig. 12 shows an AND-gate with input events A, and B, and output event Q. For an AND-gate, the output event Q only takes place when events A and B both occur at the same time.

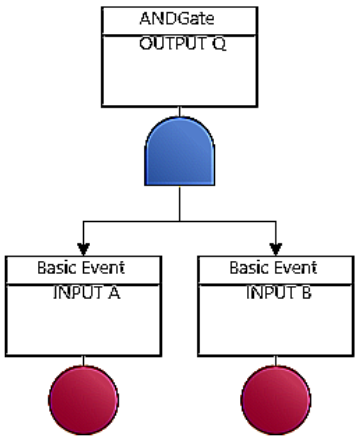

Fig. 12. Two inputs AND-gate

Boolean representation of Output Q of an AND-gate is illustrated as follows [50], [51], [53], [54]:

$$Q = A \cap B \text{ or}$$
$$= A.B \tag{12}$$

The Boolean expression for n number of input events to an AND-gate is depicted as follows [50], [51]:

$$Q = A_1 \cap A_2 \cap A_3 \cap \ldots\ldots \cap A_n$$
$$= A_1.A_2.A_3.\ldots\ldots.A_n \tag{13}$$

The probability of output Q for a two input AND-gate is presented in eq. (14) [50], [51], [54]:

$$P(Q) = P(A)P(B|A) = P(B)P(B|A) \tag{14}$$

If A and B are independent events, then

$$P(B|A) = P(B),$$
$$P(A|B) = P(A), \text{ and}$$
$$P(Q) = P(A).P(B) \tag{15}$$

Where event B completely relies on event A, that is, event A takes place, B also happens, then

$$P(B|A) = 1 \text{ and}$$
$$P(Q) = P(A)$$

5.3.3 EXCLUSIVE OR-gate Operation

The EXCLUSIVE OR-gate (XOR-gate) is used when the output event exists due to the existence of exactly one of the input events [50], [51]. Fig. 13 presents the operation of the XOR-gate.

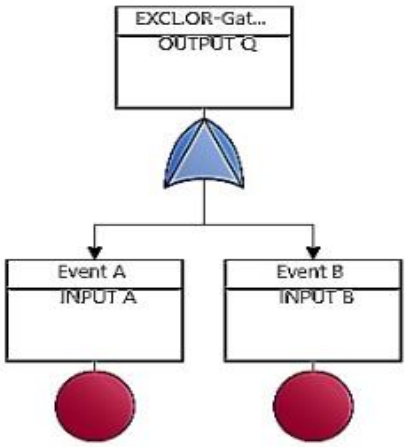

Fig. 13. XOR-gate with two inputs

The Q exists only when a single input event takes place, but not both together.

The probability Q of the above XOR-gate is depicted in eq. (16).

$$P(Q)_{XOR} = P(A) + P(B) - 2P(A \cap B) \tag{16}$$

5.3.4 PRIORITY AND-gate Operation

In the PRIORITY AND-gate, the output event occurs only if all input events occur in a specified sequence. Fig. 14 shows the operation of a typical PRIORITY AND-gate [50]. The output event Q occurs only if the input event occurs in a specific sequence with A occurs before B and both input events A and B occur.

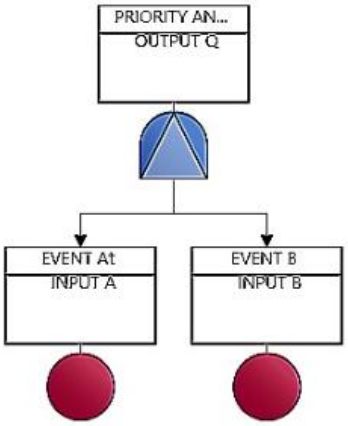

Fig. 14. PRIORITY AND-gate with two inputs

5.3.5 INHIBIT-gate Operation

The INHIBIT-gate is illustrated by a hexagon. The output takes place by a single input, but some specific criteria must be fulfilled before the input can generate the output. Fig. 15 shows a typical INHIBIT-gate with input A, and output Q. The output event Q occurs only when event A happens due to the specified condition [50].

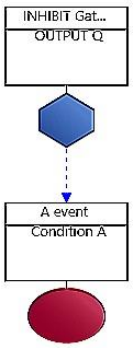

Fig. 15. Typical INHIBIT-gate with input A

5.4 Fault Tree Evaluation Techniques

The two types of outputs can be obtained from a fault tree assessment. They are [50]:

1. Qualitative results, and
2. Quantitative results.

1. Qualitative results:

Qualitative results are as follows:

(a) the minimal cut sets of the fault tree,

(b) qualitative component importance, and

(c) minimal cut sets significantly liable to common cause failures.

2. Quantitative results include the following:

(a) Absolute probabilities,

(b) quantitative importance of components and minimal cut sets, and

(c) Sensitivity and relative probability evaluations.

5.5 Minimal Cut Sets (MCS)

The major objectives of a fault tree representation by Boolean equations is that they are used to find out the "minimal cut sets (MCS)" of a fault tree. When a fault tree is assessed, the MCSs are usually found, and the failure modes of the top event are determined [50].

A MCS is the smallest combination of component failures which will cause the top failure event to occur, if they all occur [38], [43], [50]. The top event will occur, if one or more of the minimal cut sets occur. There are finite number of MCSs in a fault tree that are distinctive for the top event. For an n-component MCS, all n components in the cut set must fail for the top event failure to occur [43].

The MCS expression for the top event is illustrated as follows [38], [43], [50], [51].

$$T = M_1 \cup M_2 \cup M_3 \cup \ldots\ldots\ldots \cup M_K$$

$$= M_1 + M_2 + M_3 + \cdots \ldots \ldots + M_K \quad (17)$$

where, T is the top event and $M_1, M_2, M_3, \ldots \ldots \ldots, M_K$ are the MCSs or events.

The n-components MCS is depicted as follows [38], [43], [50], [51].

$$M_i = X_1 \cap X_2 \cap \ldots \ldots \ldots \cap X_n$$

$$= X_1.X_2 \ldots \ldots \ldots X_n \quad (18)$$

where, $X_1.X_2, \ldots \ldots \ldots X_n$ are primary events on the tree, and where M_i is not a subset of another M_j. The primary events of a certain M_i are not all contained in another M_j. If we get the top event T, then the M_is are the MCSs of the fault tree.

If A , B , and C are component failures of a fault tree and the top event comprises a one-component MCS (A) and a two-component MCS (B·C), then we can illustrate a top event expression as follows[38], [50], [51].

$$T = A + B.C$$

5.5.1 Matrix method to Obtain MCS

To obtain the Boolean Indicated Cut Sets (BICS) or MCS, each gate is randomly identified by ω and each primary event by $\emptyset$ in the fault tree [56], [57].

If $\rho_{\omega,i} = i^{th}$ input to the gate ω

$\lambda_\omega =$ number of inputs to gate ω

$x =$ the x^{th} MCS

$y =$ the y^{th} entry in a MCS

$\Delta_{x,y}=$ variable representing the y^{th} entry in the x^{th} BICS

$xmax =$ largest value of x yet used

$ymax =$ largest value of y yet used in the x^{th} MCS

The values of $\omega, \emptyset, \rho_{\omega,i}$, and λ_ω are inputs to FTA, where values of $\rho_{\omega,i}$ are discernible values

of ω and/or $\emptyset$. $\Delta_{1,1}$ is first set equal to the ω value representing the gate immediately under the TOP event. The objective is to remove all ω values from the $\Delta_{x,y}$ matrix. To accomplish this:

$$\Delta_{x,y} = \rho_{\omega,1} \quad (19)$$

For ω being an AND gate:

$$\Delta_{x,ymax+1} = \rho_{\omega,\pi} \qquad \pi = 2, 3, \ldots\ldots\ldots, \lambda_{\omega}, \quad (20)$$

Where $ymax$ is incremented when π is incremented.

For ω being an OR gate [58],

$$\left[\Delta_{xmax+1,n} \quad \begin{matrix} = \Delta_{x,n} & n=1,2,\ldots\ldots,ymax\ n\neq y \\ = \rho_{\omega,\pi} & n = y \end{matrix}\right] \quad (21)$$

$$\pi = 2, 3, \ldots\ldots, \lambda_{\omega} \quad ,$$

Where $xmax$ is incremented when π is incremented.

The processes 15,16, and 17 will be repeated until all the entries in the $\Delta_{x,y}$ matrix become values of $\emptyset$. The BICS or minimal Cut Sets are then determined.

5.5.2 Substitution Method to Determine MCS of a Fault Tree

To obtain the MCS of a fault tree, FTA is first represented by Boolean equations and then the "top-down" or "bottom-up" substitution method is performed as described below [46], [48]. The substituting and expanding Boolean expressions are used in these methods. The distributive law and the law of absorption are utilized to eliminate redundancies.

5.5.2.1 Top-down Substitution Method

First, we consider a fault tree shown in Fig. 16, then the Boolean equations are developed based on the tree structure [38], [48], [50].

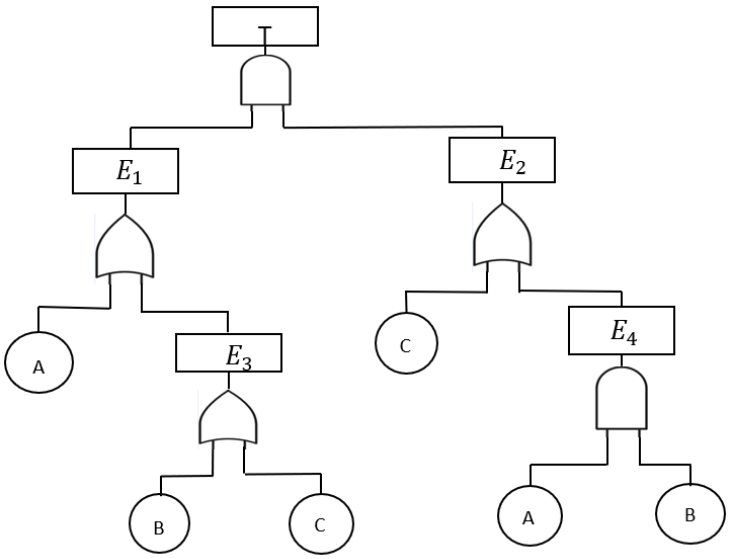

Fig. 16. The simple fault tree [48]

The equivalent Boolean equations of the tree are as follows [38], [48], [50].

$$T = E_1 . E_2$$

$$E_1 = A + E_3$$

$$E_3 = B+C$$

$$E_2 = C+E_4$$

$$E_4 = A \cdot B$$

Now, we start with the top event equation and substitute and expand that until the MCS expression for the top event is obtained. Substituting for E_1 and E_2 and expanding we get [38], [48], [50].

$$T = (A+E_3) . (C+E_4)$$

$$= (A \cdot C) + (E_3 \cdot C) + (E_4 \cdot A) + (E_3 \cdot E_4) \quad (22)$$

Substituting for E_3:

$$T = A \cdot C + (B+C) . C + E_4 \cdot A + (B+C) . E_4$$

$$= A \cdot C + B \cdot C + C \cdot C + E_4 \cdot A + E_4 . B + E_4 \cdot C.$$

Using the idempotent law, $C \cdot C = C$, then

$$T = A \cdot C + B \cdot C + C + E_4 \cdot A + E_4 \,.\, B + E_4 \cdot C.$$

But $A \cdot C + B \cdot C + C + E_4 \,.\, C = C$ by the law of absorption.

Therefore, $T = C + E_4 \cdot A + E_4 \,.\, B.$

Finally, substituting for E_4 and applying the law of absorption [38], [48], [50],

$$T = C + (A \cdot B) \cdot A + (A \cdot B) \cdot B = C + A.B \tag{23}$$

Therefore, the MCS of the top event are C and $A \cdot B$

The equivalent fault tree to the original tree is shown in Fig. 17.

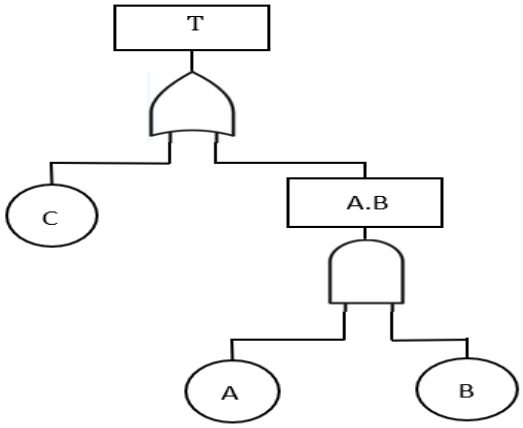

Fig. 17. Equivalent Fault Tree of Fig. 16 [48]

5.5.2.2 Bottom-up Substitution Method

The bottom-up approach uses the same substitution techniques, but in this method the process starts from the bottom and moves upward [48]. In this approach, the MCSs are found for every intermediate event as well as the top event.

The Boolean equations are presented as follows [38], [48], [50].

$$T = E_1 . E_2$$

$$E_1 = A + E_3$$

$$E_3 = B+C$$

$$E_2 = C+E_4$$

$$E_4 = A \cdot B$$

Starting from the bottom, since E_4 has only basic failures, we substitute E_4 into E_2 to obtain $E_2 = C+A \cdot B$.

The minimal cut sets of E_2 are thus C and $A \cdot B$. E_3 is already in reduced form having minimal cut sets B and C. Substituting into E_1, we obtain $E_1 = A+B+C$. So E_1 has three minimal cut sets A, B, and C. Finally, substituting the expressions for E_1 and E_2 into the equation for T, expanding and applying the absorption law, we have [38], [48], [50],

$$\begin{aligned} T &= (A+B+C) \,.\, (C+A \cdot B) \\ &= A \cdot C + A \cdot A \cdot B + B \cdot C + B \cdot A \cdot B + C \cdot C + C \cdot A \cdot B \\ &= A \cdot C + A \cdot B + B \cdot C + A \cdot B + C + A \cdot B \cdot C \\ &= C + A \cdot B. \end{aligned} \tag{24}$$

In this method, as expected, the MCSs of the top event end up to be the same as before.

5.5.3 Advantages of Minimal Cut Set (MCS) Approach

The MCS technique finds out the combinations of minimal sets of primary events that will cause the top event. The MCS method detects the notable event failure combinations and identifies the equipment for which specification modifications can eliminate or remove the unwanted combinations [50], [51]. MCSs can identify the dependencies and susceptibilities to Common Cause Failure (CCF) potentials. MCSs also furnish qualitative and quantitative information for strategic and tactical decision making [48].

5.5.4 Minimal Cut Sets Reliability Characteristics

Reliability is defined to be the probability that a component or system will perform a required function for a given period of time when used under stated operating conditions. On the other hand, Availability is defined as the probability that a component or system is performing its required function at a given point in time when used under stated operating conditions. The unavailability is the probability that the system failure does exist and numerically is equal to unity minus the availability [38], [50]. Availability is normally related to repairable systems. However, the availability is an important feature where the occurrence of the system failure is allowable for some fraction of the time [50]. For an exponential or Constant Failure Rate (CFR) model, the reliability of a component can be defined by the eq. (25).

$$R(t) = e^{-\lambda t} \tag{25}$$

Where λ is a constant failure rate of a component.

The probability that a failure occurs of a component before time t can be expressed by the eq. (26) [50].

$$F(t) = 1 - R(t) = 1 - e^{-\lambda t} \tag{26}$$

Where, a component of a system suffers its first failure within time period t, given that it is initially working.

In reliability terminology, $F(t)$ is called the component unreliability [50]. For fault tree calculation, the exponential distribution can be approximated by its first order term to simplify the calculations. Therefore, the component unreliability is approximated as the eq. (27) [50].

$$F(t) \cong \lambda t \tag{27}$$

For a repairable system, the component is repaired or replaced when it is failed. The repair or replacement operation can be characterized by the downtime of the component. The

component unavailability $q(t)$ is the probability that the component is down at time t and unable to operate if called on.

Here $1 - q(t)$ is the component availability.

It the component is not repairable, the $q(t)$ is equal to unreliability $F(t)$, and is defined by the eq. (28).

$$q(t) = F(t) \cong \lambda t \tag{28}$$

For a repairable system, the component unavailability $q(t)$ is not equal to unreliability and the information from process data requires to calculate $q(t)$ [50].

5.5.4.1 Minimal Cut Sets Unavailability for a Repairable System:

The reliability for the MCSs is assessed from the component reliability characteristics. The principal concern is the MCS unavailability for a repairable system which is illustrated by $Q(t)$ [50], [57].

$Q(t)$ =the probability that all the components in the MCS are failed at time t and unable to operate.

Since an MCS is viewed as a particular failure mode of the system, $Q(t)$ is defined as:

$Q(t)$ = the probability that the system is down at time t due to the particular MCS.

$Q_i(t)$ is the unavailability for minimal cut set i.

If the component failures in a MCS are independent, the unavailability of the MCS is expressed as given by eq. (29) [50], [57].

$$Q_i(t) = q_1(t).\, q_2(t) \ldots\ldots q_{n_i}(t) = \prod_{i=1}^{n_i} q_i(t) \tag{29}$$

Where, $q_1(t), q_2(t)$, etc. are the unavailabilities of the component in the particular MCS and n_i is the number of components in the cut set.

5.5.4.2 Minimal Cut Set Occurrence Rate W(t)

The number of system failures and the probability of no system failure is important for a running system. The MCS failure rate (that is, failure per unit time) can be calculated, and it is denoted by $W(t)$ [50], [57]. Then, by definition, $W(t)\Delta t$ is the probability that the MCS failure takes place between time t to $t+\Delta t$, given that MCS failure does not exist at time t.

If we consider all the MCSs of the tree, then $W_i(t)$ refers to the occurrence rate of MCS i. If the component failures are independence, $W_i(t)$ is illustrated as eq. (30) [50], [57].

$$W_i(t)\,\Delta t = = \sum_{i=1}^{n_i} w_i(t)\Delta t \prod_{\substack{l=1 \\ l\neq j}}^{n_i} q_l(t) \tag{30}$$

If we cancel Δt from above equation, then the MCS occurrence rate, $W_i(t)$ is illustrated as eq. (31) [50], [58].

$$W_i(t) = \ = \sum_{i=1}^{n_i} W_i(t) \prod_{\substack{l=1 \\ l\neq j}}^{n_i} q_l(t) \tag{31}$$

5.5.4.3 Expected Number of Failures

The expected number of failures $N_i(t_1, t_2)$ of minimal cut set i for a period time t_1 to t_2 is defined as the following eq. (32) [50], [57].

$$N_i(t_1, t_2) = \int_{t_1}^{t_2} W_i(t)\, dt$$

$$= \sum_{i=1}^{n_i} W_i(t) \prod_{\substack{l=1 \\ l\neq j}}^{n_i} q_l(t) \tag{32}$$

If $W_i(t)$ is constant, $W_i(t) = W_i$, then $N_i(t_1, t_2)$, is defined as follows:

$$N_i(t_1, t_2) = (t_2 - t_1)\, W_i$$

5.6 System Top Event Reliability Characteristics

5.6.1 System Unavailability for a Repairable System

The unavailability of the system is the probability that the system does not function at a given point in time under specified conditions. For a repairable system, the unavailability (Q),

is denoted by the eq. (33) [38].

$$Q = \frac{MTTR}{MTTR+MTBF} \tag{33}$$

where $MTTR$=Mean time to repair, and

$MTBF$ =Mean time between failures.

The unavailability can also be expressed as the eq. (34).

$$Q = \frac{\lambda}{\lambda+\mu} \tag{34}$$

where λ, and μ are the failure and repair rates, respectively.

Mean Unavailability:

The mean unavailability is defined as the ratio of mean downtime to total time.

The system unavailabilty calculation for a repairable system using minimal cut sets:

Q_i(t) is the unavailability for minimal cut set i, therefore [50], [57], [58],

$$Q_i(t) = q_1(t).q_2(t) \ldots\ldots q_{n_i}(t) = \prod_{i=1}^{n_i} q_i(t) \tag{35}$$

Where, $q_1(t), q_2(t)$, etc. are the unavailabilities of the component in the particular minimal cut set i and n_i is the number of components in the cut set.

$Q_s(t) =$ the probability that the system is down at time t and unable to function.

The general equation for system unavailability, $Q_s(t)$ for a repairable system can be illustrated by eq. (36) [57], [58].

$$Q_s(t) = \sum_{i=1}^{N} Q_i(t) - \sum_{i=2}^{N} \sum_{j=1}^{i-1} \prod^{+i,j} q(t) + \cdots . + (-1)^{N-1} \prod^{+i,j} q(t) \tag{36}$$

If we consider two or more minimal cut sets failure do not occur at a time, the system unavailability $Q_s(t)$ can be approximated as the eq. (37) [50],[57], [58].

$$Q_s(t) \cong \sum_{i=1}^{N} Q_i(t) \tag{37}$$

where N is the number of minimal cut sets in the tree.

The system unavailability $Q_s(t)$ is time independent and a fixed value Q_s, when all the component failures are cyclic or repairable and their unavailability are fixed value.

5.6.2 System Failure Occurrence Rate, $W_s(t)$

For the running system, the $W_s(t)$ is important.

$W_s(t)\Delta t$ =the probability that the system fails in time t to $t+\Delta t$ [50], [57], [58]

Therefore, $W_s(t)$ can be denoted as eq. (38) [57].

$$W_s(t) = \frac{\sum_{i=1}^{N} W_i(t)}{\prod_{i=1}^{N}(1-Q_i(t))} \tag{38}$$

If we consider the system failure occurs when one or more of the minimal cut sets occur, then, $W_s(t)$, can be expressed as shown in eq. (39) [50], [57], [58].

$$W_s(t) = \sum_{i=1}^{N} W_i(t) \tag{39}$$

5.6.3 Expected Number of System Failure

Number of failures:

The number of failures of a repairable system over a specific period of time is one of the critical system reliability indices. If the managers and engineers can predict the number of failures of a system, they can the take necessary actions to prevent those potential failures. The equation for expected number of failures of a system from time 0 to t is illustrated by eq. (40).

$$E\big(N(t)\big) = \int_0^t \lambda(t)dt \tag{40}$$

where λ is the failure rate of the system.

The expected number of system failures is also evaluated by MCSs.

The expected number of system failure $N_s(t_1, t_2)$ in time $t_1$to t_2 is defined by the eq. (41) [50].

$$N_s(t_1, t_2) = \int_{t_1}^{t_2} W_s(t)\, dt \tag{41}$$

The expected number of system failure in time t, $N_s(t)$ is illustrated by the eq. (42) [50][57].

$$N_s(0, t) = \int_0^t W_s(t')\, dt' \tag{42}$$

When, $W_s(t)$ is a constant value of W_s, and when all the component failures are cyclic or repairable and their unavailabilities are fixed values, the expected number of system failures $N_s(t_1, t_2)$ in time t_1 to t_2, is W_s times the interval $t_2 - t_1$.

The system unavailability $Q_s(t)$, the system failure occurrence rate $W_s(t)$, and the expected number of system failures $N_s(t_1, t_2)$ present system failure data.

5.7 Minimal Cut Sets and Component Importance

5.7.1 Minimal Cut Sets and Component Importance in terms of System Unavailability

The minimal cut set importance is defined as the fraction of system failure probability that is contributed by a particular minimal cut set. The minimal cut set importance and the component importance are assessed with respect to the system unavailability, $Q_s(t)$, or the system failure occurrence rate, $W_s(t)$, as shown later in eqs. (39) and (41), respectively.

Let $E_i(t)$ be the importance of minimal cut set i at time t and $e_k(t)$ be the importance of component k at time t. With respect to system unavailability, the $E_i(t)$ and $e_k(t)$ are then defined by the eq. (43) and eq. (44), respectively [50].

$$E_i(t) = \frac{Q_i(t)}{Q_s(t)} \tag{43}$$

$$e_k(t) = \frac{\sum_{k\ in\ i} Q_i(t)(t)}{Q_s(t)} \tag{44}$$

Where,

$Q_i(t)$ is the unavailability of MCS_i and $Q_s(t)$ is the system unavailability.

$e_k(t)$ is the fraction of system unavailability contributed by the failure of component k.

For a repairable system where the component unavailability is constant, $E_i(t)$ and $e_k(t)$ are fixed and time independent. Therefore $E_i(t) = E_i$ and $e_k(t) = e_k$. Hence, the minimal cut

set and component importance can be categorized from highest to lowest value without any time considerations [50].

5.7.2 Minimal Cut Sets and Component Importance in terms of System Failure Occurence Rate $W_s(t)$

In terms of the system failure occurrence rate $W_s(t)$, the minimal cut set importance $\widehat{E_i}(t)$ is defined by the eq. (45) [50]:

$$\widehat{E_i}(t) = \frac{W_i(t)}{W_s(t)} \tag{45}$$

and the component importance $\widehat{e_k}(t)$ are defined by the eq. eq. (46)

$$\widehat{e_k}(t) = \frac{\sum_{k\ in\ i} W_i(t)}{W_s(t)} \tag{46}$$

$\widehat{E_i}(t)$ and $\widehat{e_k}(t)$ are fixed values and can be categorized by the largest to smallest when the component features are fixed values [50].

5.8 Reliability Characteristics Equations

5.8.1 Summary of Reliability Equations

A summary of the reliability equations is shown in Table 1.

Table 1. Summary of Reliability Characteristics Equations.

	Unavailability	**Failure Occurrence Rate**
Minimal Cut Sets	$Q_i(t) = q_1(t).q_2(t)$ $\ldots\ldots q_{n_i}(t)$ $= \prod_{i=1}^{n_i} q_i(t)$ where, $q_1(t), q_2(t),$ etc. are the component unavailabilities contained in	$W_i(t) = q_2(t).q_3(t) \ldots\ldots$ $q_{n_i}(t)W_1(t) + q_1(t)q_3(t)$ $\ldots\ldots q_{n_i}(t)W_2(t) + q_1(t)q_2(t)$ $\ldots\ldots q_{n_i}(t)W_3(t) + \cdots \ldots\ldots\ldots\ldots$

	a specific MCS, and n_i is the number of components in MCS.	$+q_1(t)q_2(t) \dots q_{n_i}(t)W_{n_i}(t))$ $= \sum_{i=1}^{n_i} W_i(t) \prod_{\substack{l=1 \\ l \neq j}}^{n_i} q_l(t)$
System	$Q_s(t) = \sum_{i=1}^{N} Q_i(t)$ where $N = 1, \dots, N$ are number of minimal cut sets	$W_s(t) = \sum_{i=1}^{N} W_i(t)$

5.8.2 Summary of Importance Measures

Reliability importance measures identify the events leading to the most system performance improvement. Importance measures significantly improve system reliability by ranking the events of failure in the order of reduced likelihood of occurrence. The marginal, critical, diagnostic, risk reduction, and risk achievement are the importance measures of events and are used to figure out risks [59].

5.8.2.1 Marginal Important Measure (MIM)

The Marginal Important Measure determines the failure probability of the top event due to any event. It is evaluated by the deference of the probability of the top event *(E)* failure when an event *A* does occur and the probability of the top event *(E)* failure when the event *A* does not occur.

Marginal Importance Measure (MIM) is defined as follows [59].

$$MIM = P(E|P(A)=1)-P(E|P(A)=0)$$

The MIM shows how event A increases the probability of a top event E.

5.8.2.2 Criticality Importance Measure (CIM)

Criticality is the quality, state, or degree of importance of the equipment, and it is used in operational decision-making and asset replacement processes. The CIM is a modification of MIM that also considers the probability of event A.

Criticality Importance Measure (CIM) is expressed as follows [59].

$$CIM = \text{Marginal Importance Measure} * P(A)/P(E)$$

$$= MIM * P(A)/P(E)$$

where $P(E)$ is the probability of the top event E due to an event A. It helps to figure out the faults that frequently occur.

5.8.2.3 Risk Reduction Worth (RRW)

The RRW measures the reduction in the probability of the top event if any event does not occur. RRW also represents the Top Decrease Sensitivity [43]. RRW gives the maximum reduction in the probability of the top event due to any system equipment upgrades. The absolute value and relative value of RRW can be measured for each event.

Specifically, RRW is defined to be the ratio of the probability of top event E and the probability of top event E given event A does not occur. The expression of RRW is as follows [59].

$$RRW = P(E) \; / \; P(E|P(A) = 0)$$

5.8.2.4 Diagnostic Importance Measure (DIM)

DIM is the fraction of the top event E probability when the event A occurs times the probability of event A divided by the probability of the top event.

Diagnostic Importance Measure (DIM) is defined as follows [59].

$$DIM = P(A) * P(E|P(A)=1)/P(E).$$

5.8.2.5 Risk Achievement Worth (RAW)

RAW determines the increment of the top event probability when any event occurs. It is also known as the Top Increase Sensitivity [42]. It identifies where preventive work is required to maintain system continuity.

RAW is defined by the ratio of the probability of top even E when event A does not occur, and the probability of E [59].

$$RAW = P(E|P(A) = 0)/\ P(E)$$

5.9 Quantitative Importance Equations in Terms of Minimal Cut Sets

A summary of quantitative importance measures with respect to minimal cut sets and system unavailability is provided in Table 2.

Table 2. Summary of Quantitative Importance Measures

	i^{th} Minimal Cut set importance	**k^{th} Component Importance**
In Terms of System Unavailability	$E_i(t) = \frac{Q_i(t)}{Q_s(t)}$	$e_k(t) = \frac{\sum_{k\ in\ i} Q_i(t)}{Q_s(t)}$
In Terms of System Failure Occurrence Rate	$\widehat{E_i}(t) = \frac{W_i(t)}{W_s(t)}$	$\widehat{e_k}(t) = \frac{\sum_{k\ in\ i} W_i(t)}{W_s(t)}$

6 FTA SIMULATION MODELS

To investigate the reliability of HVAC, HVDC, and LFAC transmission topologies, the FTA module of the Relyence Corporation reliability software platform has been used [59]. As stated earlier, an FTA model is a graphical design technique widely used for measuring reliability, the probability of failure, and the system's safety [21]. This model is an analytical method for calculating the system reliability indices using a direct numerical method [22]. The FTA diagram comprises Boolean logic gates, such as AND, OR, XNOR, XOR etc. which are connected to represent various system event interactions.

Commonly used terminology associated with FTA are Events, Logic gates, Risk measures, Important measures, and Minimal cut sets. The top event is the undesired output, or the failure of the whole system. The basic and intermediate events are linked to the top event through various gates which contribute to the top event or cause the system's failure. These actions from the chain of events or failure combinations. The fixed failure and repair rates of basic level events are used to figure out the probability of the top event, and the logic gates are used to define the conditions of a set of events that result in a specific output. An essential task of FTA is to identify the minimal cut sets, which are the sets of events that would result in the topmost event. The minimal cut sets are the combination of minimum events that will trigger the topmost undesirable output and are used to identify the system's vulnerability [38].

The offshore wind power transmission system's failure is the top event for HVAC, HVDC, and LFAC systems, each of which has various system component failures. The HVAC transmission system is composed of the wind turbine (WT), in-farm AC (IFAC) line, small switch (SSW), small transformer (ST), large switch (LSW), large transformer (LT), AC bus, and high voltage AC (HVAC) transmission line. The HVDC transmission system is comprised

of the wind turbine (WT), in-farm AC line (IFAC), small switch (SSW), small transformer (ST), large switch (LSW), large transformer (LT), AC/DC converter, DC bus, DC/AC converter, and high voltage DC (HVDC) transmission line. The LFAC Transmission system is comprised of the wind turbine (WT), in-farm DC (IFDC) line, small switch (SSW), small transformer (ST), AC/DC converter, large switch (LSW), DC bus, large transformer (LT), LFAC transmission line, DC/AC converter, Cycloconverter, 20 Hz interconnection line, and 20 Hz Transformer.

6.1 HVAC FTA Simulation Model

Basic events, transfer functions, AND-gates, and OR-gates have been used to implement the simulation models of an HVAC transmission system. A basic event initiates the fault or failure event and is represented by a circle. A transfer function is represented by a triangle and indicates a transfer condition to a subtree. The OR-gate is used when an output occurs if one of the inputs occurs, and the AND-gate is used when an output occurs if all inputs occur. The initial events of an HVAC transmission system are Wind Turbine (WT) failure, Small Transformer (ST) failure, Small Switches (SSW) failure, in-farm AC (IFAC) transmission line failure, large switch failure, large transformer failure, AC bus failure, and high voltage AC transmission line failure. In HVAC system, the small switch is the CT, PT, breaker, and all other small associated components with windfarms and large switch is the CT, PT, breaker, and associated component with AC bus. The small transformer is the transformer which is linked with windfarms, and large transformer is the transformer which is linked with AC bus.

In this model, Wind Turbine (WT) failure, Small Transformer (ST) failure, Small Switches (SSW) failure, and in-farm AC (IFAC) transmission line failure are connected through OR-gate to define a windfarm failure, since if any of these components fail, the windfarm will fail. In this model, ten windfarms are connected through an AND-gate for

feeder failure, since if any of the windfarms fails, the feeder itself will not fail. The three feeders of the system are connected through transfer functions for feeder system failure. These three transfer functions are connected through the AND-gate, since if any of the feeders fails, the feeder system will not fail. The AC bus, large switch (LSW), and feeder system are connected through the OR-gate, since if any of the components fail, the AC bus will fail. HVAC transmission line failure, large transformer (LT) failure, and AC bus failure are connected through the OR-gate, since if any of the components fails, the HVAC transmission system will fail. The simulation model of the HVAC transmission system is illustrated in Figs. 18, 19, and 20.

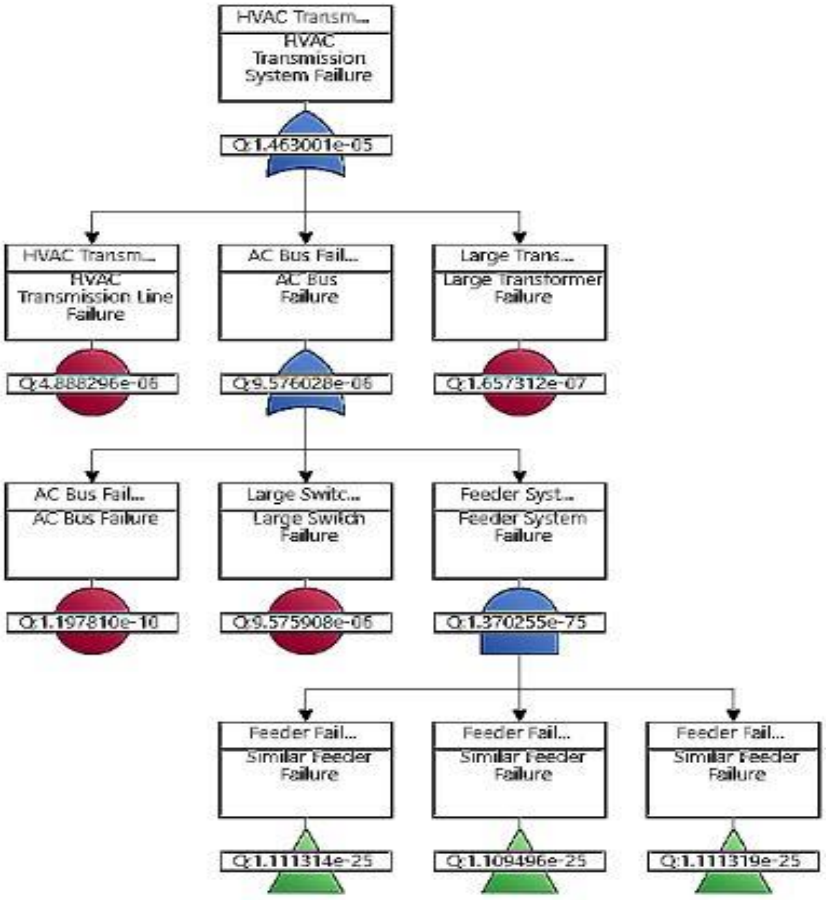

Fig. 18. HVAC Transmission System Fault Tree.

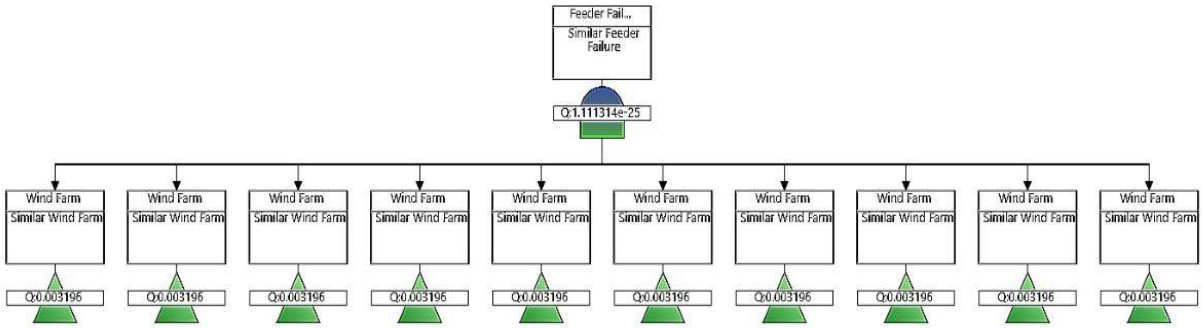

Fig. 19. HVAC Transmission System Feeder Fault Tree.

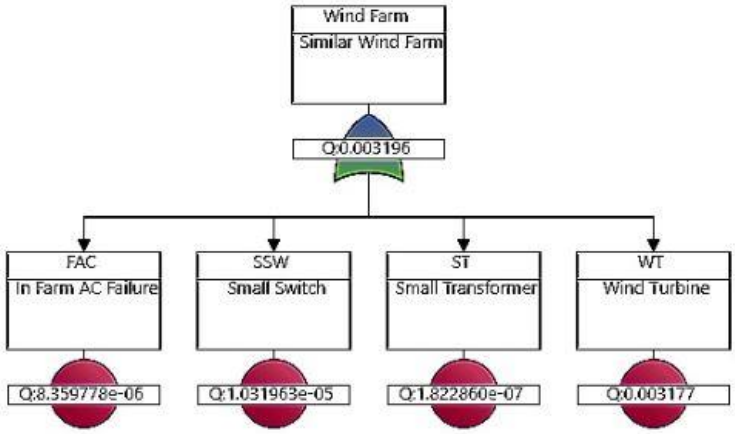

Fig. 20. HVAC Single Windfarm Failure Model

6.2 HVDC FTA Simulation Model

The initial events of the HVDC simulation model are Wind Turbine (WT) failure, Small Transformer (ST) failure, Small Switches (SSW) failure, in-farm AC (IFAC) transmission line failure, large switch (LSW) failure, large transformer (LT) failure, AC/DC converter failure, DC/AC inverter failure, DC bus failure, and high voltage DC (HVDC) transmission line failure. In HVDC system, the small switch comprises the Current transformer (CT), Potential Transformer (PT), breaker, and all other small components associated with windfarms and large switch comprises the CT, PT, breaker, and other components associated

with DC bus. The small transformer is the transformer which is linked to windfarms, and large transformer is the transformer which is linked to DC bus.

Wind Turbine (WT) failure, Small Transformer (ST) failure, Small Switch (SSW) failure, and in-farm AC (IFAC) transmission line failure are connected through the OR-gate to define the windfarm failure, since if any of these components fail, the windfarm will fail. In this model, ten wind farms are connected through the AND-gate for feeder failure, since if any of the wind farms fails, the feeder will not fail. The three feeders of the system are connected through transfer functions for feeder system failure. Three transfer functions are connected through the AND-gate, since if any of the feeders fails, the feeder system will not fail. DC bus, large switch, AC/DC converter, and feeder system are connected through the OR-gate, since if any of these components fails, the DC bus will fail. HVDC transmission line failure, large transformer (LT) failure, DC/AC converter failure, and DC bus failure are connected through the OR-gate, since if any of these components fails, the HVDC transmission system will fail. The simulation model of the HVDC transmission system is depicted in Figs. 21, 22, and 23.

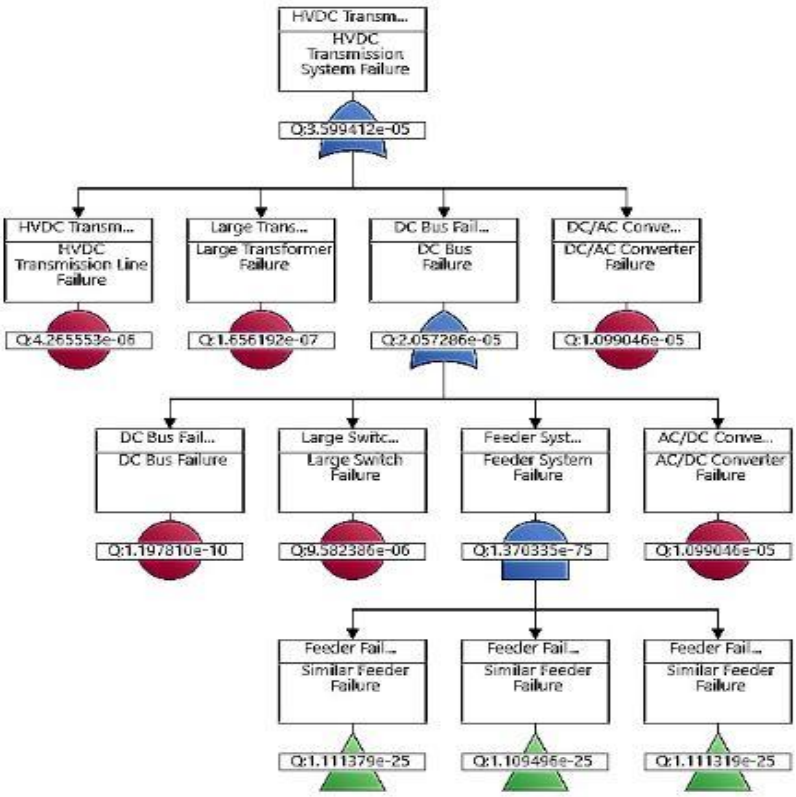

Fig. 21. HVDC Transmission System Fault Tree.

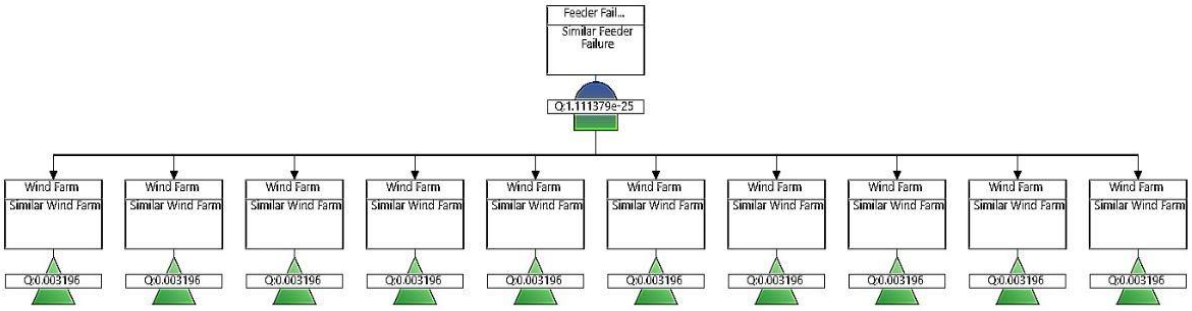

Fig. 22. HVDC Transmission System Feeder Fault Tree

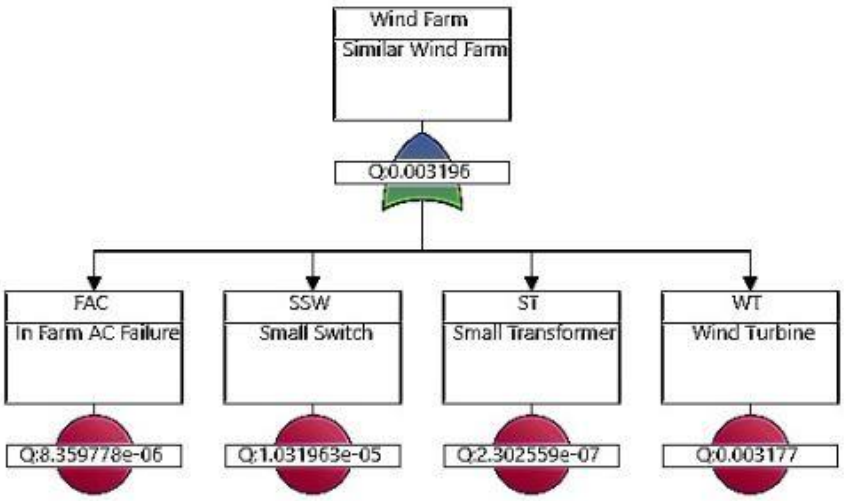

Fig. 23. HVDC Single Windfarm Failure Model

6.3 LFAC FTA Simulation Model

The initial event of the simulation model are Wind Turbine (WT) failure, small AC-DC Converter failure, Small Transformer (ST) failure, small Switches (SSW), and in farm DC (IFDC) transmission line failure. If any of the above five items fails, the wind farm will fail. So for building a simulation model, the OR-gate has been used for these five items.

Since if any of the ten windfarms fails, the individual feeder will not fail, the ten wind farms are connected through an AND-gate in the model. The three feeders of the system are connected in the simulation model through the transfer function. When all the feeders fail, the feeder system also will fail, so the three feeders of the system are connected through an AND-gate in the model. If any of the DC bus, large switch, Current Transformer (CT), Potential Transformer (PT), breakers, and all other equipment associated with the bus and feeder system fail, the DC bus will fail. So, the DC bus failure, large switch (LSW) failure, and feeder system failure are connected through the OR-gate in the model. If any of the LFAC transmission line, large transformer, DC bus, DC-AC converter, cycloconverter, interconnection line and 20 Hz transformer fail, the

LFAC transmission system will fail. So, all these items are connected through an OR-gate in the model. The FTA simulation model of the LFAC transmission system is shown in Figs. 24, 25, and 26.

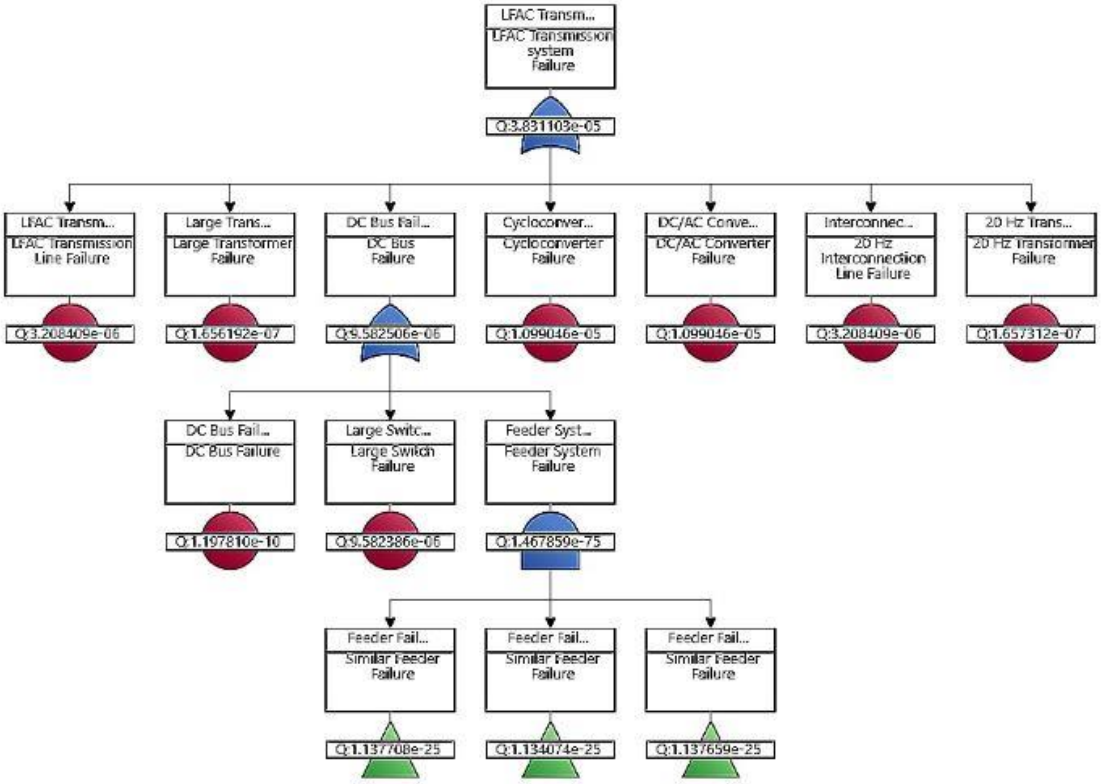

Fig. 24. LFAC Transmission System Fault Tree.

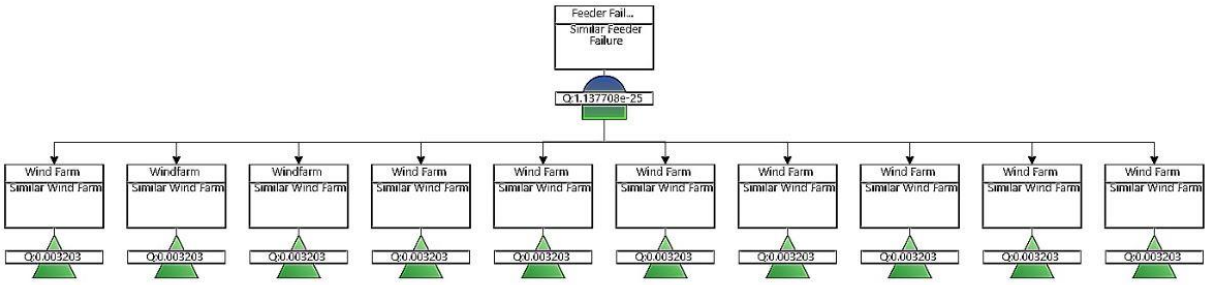

Fig. 25. LFAC Single Feeder Failure Model.

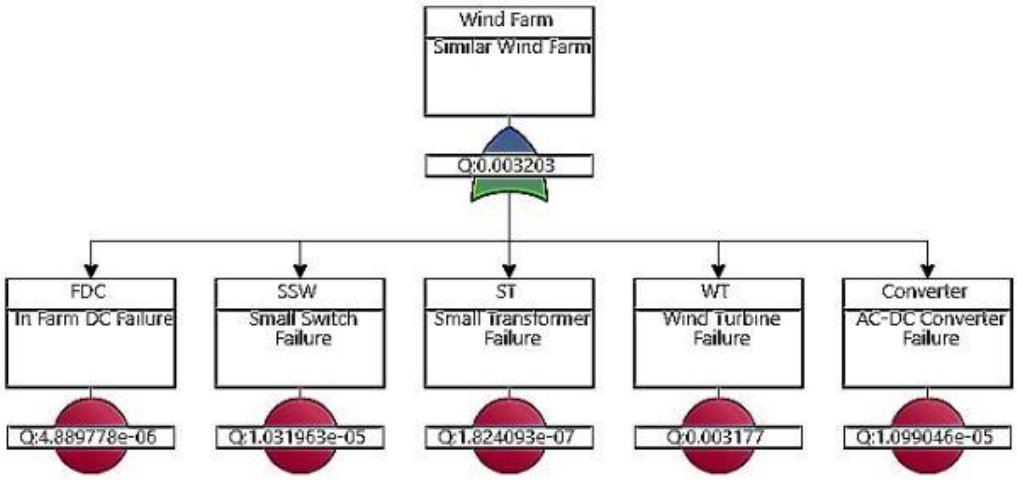

Fig. 26. LFAC Single Windfarm Failure Model.

6.4 Reliability Model Parameters

The reliability model parameters of the simulation models for HVAC, HVDC, and LFAC transmission system topologies are shown in Table 3 and are drawn from [10]. The values of the failure and repair rates are per year.

Table 3. Failure rate of the system components

Components	**Typical Value of Failure Rate per year**	**Typical value of Repair Rate per year**
Wind Turbine (WT)	$\lambda_{WT} = 0.402$	$\mu_{WT} = 69.546$
Small Switch (SSW)	$\lambda_{sSW} = 0.0061$	$\mu_{sSW} = 14.84$
Small Transformer (ST)	$\lambda_{sT} = 0.003$	$\mu_{sT} = 0.533$
Large AC/DC Converter	$\lambda_{\frac{lAC}{DC}} = 0.0298$	$\mu_{\frac{lAC}{DC}} = 3.233$
DC Bus	$\lambda_{\mathrm{DCB}} = 0.000125$	$\mu_{\mathrm{DCB}} = 0.0084$
Large Switch (LSW)	$\lambda_{\mathrm{lSw}} = 0.0096$	$\mu_{\mathrm{lSw}} = 8.75$
60 Hz HVAC transmission line	$\lambda_{60\mathrm{AC}} = 0.0141$	$\mu_{60\mathrm{AC}} = 3.04$
Large Transformer (LT)	$\lambda_{\mathrm{lT}} = 0.0032$	$\mu_{\mathrm{lT}} = 0.454$

DC/AC Converter	$\lambda_{\frac{DC}{AC}} = 0.0298$	$\mu_{\frac{DC}{AC}} = 3.233$
HVDC transmission line	$\lambda_{DC} = 0.0123$	$\mu_{DC} = 3.04$
20 Hz LFAC transmission line	$\lambda_{20AC} = 0.0075$	$\mu_{20AC} = 3.75$
In farm AC transmission line (FAC)	$\lambda_{FAC} = 0.0189$	$\mu_{FAC} = 3.88$
In farm DC transmission line (FDC)	$\lambda_{FDC} = 0.0141$	$\mu_{FDC} = 3.04$
60 Hz AC Bus	$\lambda_{ACB} = 0.000125$	$\mu_{ACB} = 0.0084$
Cyclo-converter	$\lambda_{conv} = 0.0298$	$\mu_{conv} = 3.233$
20 Hz Interconnection line	$\lambda_{Inter20} = 0.0075$	$\mu_{Inter20} = 3.75$
20 Hz transformer	$\lambda_{20T} = 0.0032$	$\mu_{20T} = 0.454$

7 SIMULATION RESULTS AND ANALYSIS

7.1 Time-based Results of HVAC, HVDC, and LFAC Transmission Topologies

7.1.1 Number of Failures

The number of failures of different systems with respect to time are illustrated in Table 4 and Fig. 27.

Table 4. Number of failures of the systems

Time (hour)	HVAC Transmission System	HVDC Transmission System	LFAC Transmission System
0	0	0	0
1000	0.0031	0.0097	0.0103
2000	0.0062	0.0193	0.0207
3000	0.0092	0.0290	0.0310
4000	0.0123	0.0387	0.0414
5000	0.0154	0.0484	0.0517
6000	0.0185	0.0581	0.0621
7000	0.0216	0.0678	0.0724
8000	0.0247	0.0774	0.0828
9000	0.0277	0.0871	0.0931
10000	0.0308	0.0967	0.1035

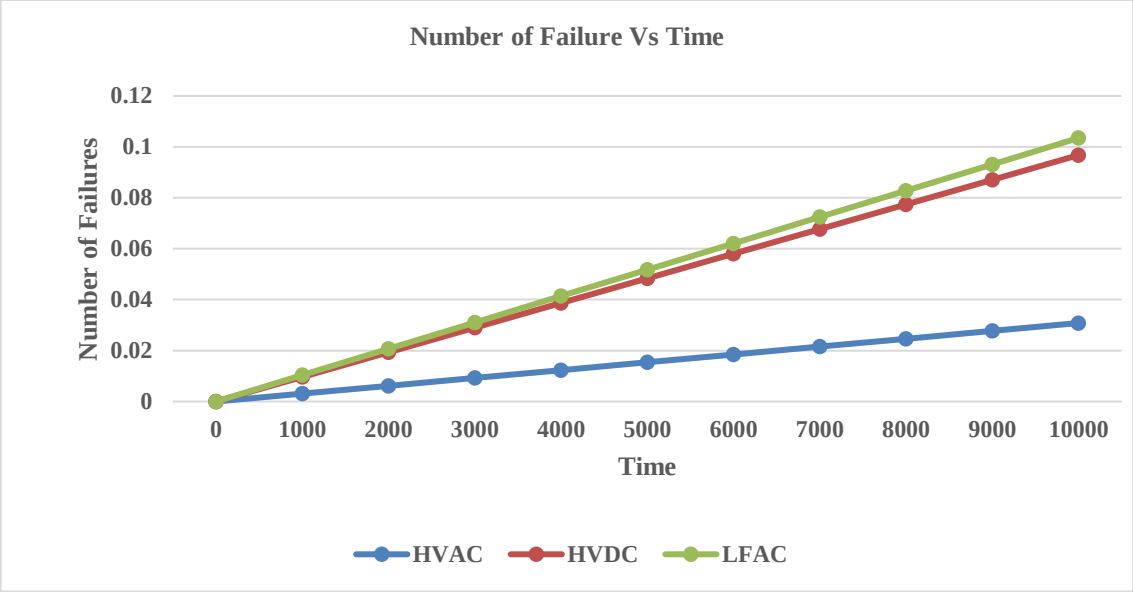

Fig. 27. Number of Failures Vs. Time.

Fig. 27 illustrates the number of failures of the HVAC, HVDC, and LFAC transmission systems increasing with time. At 10,000 hours, the number of failures of the HVAC, HVDC, and LFAC transmission systems are 0.0308, 0.0967, and 0.1035, respectively, where the number of failures of the HVAC transmission system is lowest among the three transmission systems.

7.1.2 Mean Unavailability:

The mean unavailability of different systems with respect to time are presented in Table 5, and Fig. 28.

Table 5. Mean unavailability of the systems.

Time (hour)	HVAC Transmission	HVDC Transmission	LFAC Transmission
0	0	0	0
1000	1.453E-05	3.582E-05	3.813E-05

2000	1.458E-05	3.591E-05	3.822E-05
3000	1.459E-05	3.594E-05	3.825E-05
4000	1.460E-05	3.595E-05	3.827E-05
5000	1.461E-05	3.596E-05	3.827E-05
6000	1.461E-05	3.596E-05	3.828E-05
7000	1.461E-05	3.597E-05	3.828E-05
8000	1.462E-05	3.597E-05	3.829E-05
9000	1.462E-05	3.597-05	3.829E-05
10000	1.462E-05	3.598E-05	3.829E-05

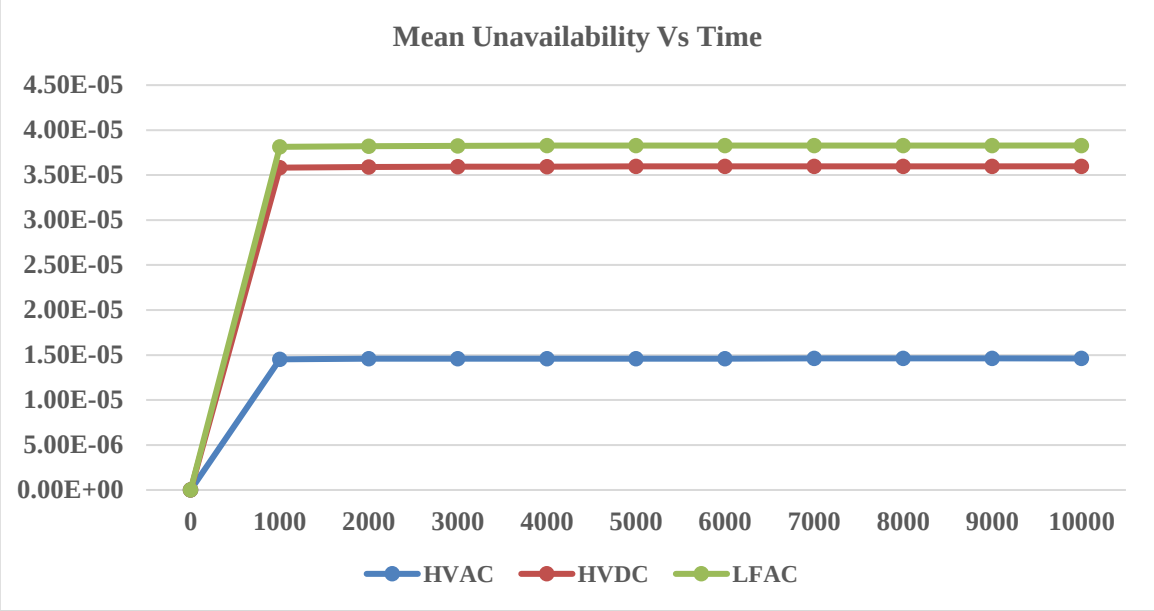

Fig. 28. Mean Unavailability Vs Time

Table 5 and Fig. 28 demonstrate that the mean unavailability of HVAC, HVDC, and LFAC transmission systems. As shown, at 10,000 hours, the mean unavailability of the HVAC, HVDC, and LFAC transmission systems are 1.462E-05, 3.598E-05, and 3.829E-05, respectively, where the mean unavailability is lowest in for HVAC transmission system

among the three transmission systems. Since all the systems are repairable, the system unavailability does not significantly rise with time.

7.2 Cut Sets Probability of System Components

The cut set probability of different components of the HVAC, HVDC, and LFAC transmission systems are illustrated in Table 6.

Table 6. Cut Sets probability of the system components

Event	Cut Sets Probability of HVAC System	Cut Sets Probability of HVDC System	Cut Sets Probability of LFAC System
Large Switch Failure (LSW)	9.576E-06	9.582E-06	9.582E-06
HVAC Transmission Line	4.888E-06		
HVDC Transmission Line		4.265E-06	
LFAC Transmission Line			3.208E-06
Large Transformer (LT)	1.657E-07	1.656E-07	1.656E-07
AC Bus	1.198E-10		
DC Bus		1.198E-10	1.198E-10
AC/DC Converter		1.099E-05	
DC/AC Converter		1.099E-05	1.099E-05
Cycloconverter			1.099E-05
20 Hz Interconnection Line			3.208E-06
20 Hz Transformer			1.657E-07

Table 6 shows that the large switch has the maximum cut set probability in HVAC; the AC/DC and DC/AC converter have the maximum cut set probability in the HVDC transmission system; and the DC/AC converter and Cycloconverter have the maximum cut set probability in the LFAC transmission system: 9.576E-06, 1.099E-05, and 1.099E-05, respectively. The cut set probability of the HVAC, HVDC, and LFAC transmission lines are 4.888E-06, 4.265E-06, and 3.208E-06, respectively. The LFAC transmission line has the lowest cut set probability among the three transmission lines.

7.3 Criticality Indices of System Components failures

Criticality indices of the HVAC, HVDC, and LFAC transmission system failures, and comparison of criticality indices of three transmission systems failures are shown in Tables 7, 8, 9, and 10, respectively.

Table 7. Criticality indices of the HVAC Transmission System failures

Event	Criticality
AC Bus failure	8.187E-06
HVAC Transmission Line Failure	0.334
Large Switch Failure (LSW)	0.654
Large Transformer (LT)	0.011

Table 8. CriticalityIindices of the HVDC transmission System failures

Event	Criticality
DC Bus failure	3.328E-06
HVDC Transmission Line Failure	0.118
Large Switch Failure (LSW)	0.266
Large Transformer (LT)	0.005

AC/DC Converter	0.305
DC/AC Converter	0.305

Table 9. Criticality Indices of LFAC transmission system failures

Event	Criticality
20 HZ TF	0.004
Converter (DC/AC)	0.287
Cycloconverter	0.287
DC Bus	3.1E-06
Inter Connection Line	0.084
Large Switch Failure (LSW)	0.250
Large Transformer (LT)	0.004
LFAC Transmission Line	0.084

Table 10. Comparison of Criticality Indices of three transmission systems failures

Event	Criticality		
	HVAC	**HVDC**	**LFAC**
HVAC Transmission Line Failure	0.334		
HVDC Transmission Line Failure		0.118	
LFAC Transmission Line			0.084

Large Switch Failure (LSW)	0.654	0.266	0.250
Large Transformer (LT)	0.011	0.005	0.004
AC Bus failure	8.187E-06		
DC Bus failure		3.328E-06	3.1E-06
AC/DC Converter		0.305	
DC/AC Converter		0.305	0.287
20 HZ TF			0.004
Cycloconverter			0.287
Inter Connection Line			0.084
LFAC Transmission Line			0.084

Table 7 shows the HVAC system has the lowest criticality index for its AC bus failures and the highest criticality index for its large switch failures, compared to other components. Table 8 shows the HVDC system has the lowest criticality index for its DC bus failures and the high criticality index for its AC/DC and DC/AC converter failures, compared to other components. Table 9 shows the LFAC system has the lowest criticality for its DC bus failures and high criticality indices for its DC/AC converter and Cycloconverter failures, compared to other components.

7.4 Risk Reduction Worth (RRW) Indices of System Components

Risk Reduction indices of the HVAC, HVDC, and LFAC Transmission system failures, and comparison of RRW of three transmission systems failures are presented in Tables 11, 12, 13, and 14, respectively.

Table 11. Risk Reduction Idices of the HVAC transmission system failures

Event	Risk Reduction
AC Bus failure	1.000
HVAC Transmission Line Failure	1.502
Large Switch Failure (LSW)	2.895
Large Transformer (LT)	1.011

Table 12. Risk Reduction Indices of the HVDC transmission System failures

Event	Risk Reduction
DC Bus failure	1.000
HVDC Transmission Line Failure	1.134
Large Switch Failure (LSW)	1.363
Large Transformer (LT)	1.005
AC/DC Converter	1.439
DC/AC Converter	1.439

Table 13. Risk Reduction Indices of the LFAC transmission system failures

Event	Risk Reduction
20 HZ Transformer	1.004
Converter (DC/AC)	1.402
Cycloconverter	1.402
DC Bus	1.000
Inter Connection Line	1.091
Large Switch Failure (LSW)	1.333
Large Transformer (LT)	1.004

LFAC Transmission Line	1.091

Table 14. Comparison of Risk Reduction Indices of three transmission systems failures

Event	Risk Reduction		
	HVAC	**HVDC**	**LFAC**
HVAC Transmission Line Failure	1.502		
HVDC Transmission Line Failure		1.134	
LFAC Transmission Line			1.091397
Large Switch Failure (LSW)	2.895	1.005	1.333
Large Transformer (LT)	1.011	1.005	1.004
AC Bus failure	1.000		
DC Bus failure		1.000	1.000
AC/DC Converter		1.439	
DC/AC Converter		1.439	1.402
20 HZ TF			1.004
Cycloconverter			1.402
Inter Connection Line			1.091

Tables 11 shows that for the HVAC system, the AC bus has the lowest risk reduction, and the large switch has the highest risk reduction, compared to other components. Table 12 shows that for the HVDC system, the DC bus has the lowest risk reduction, and AC/DC and DC/AC converters have the highest risk reductions, compared to other components. Table 13 shows that

for the LFAC system, the DC bus has the lowest risk reduction, and DC/AC converter and Cycloconverter have the highest risk reductions, compared to the other components.

7.5 Failure Probability of System Components

The failure probability of HVAC, HVDC, and LFAC systems components are shown in Table 15.

Table 15. Component Failure probability of the three transmission systems

Event	Failure Probability of HVAC System	Failure Probability of HVDC System	Failure Probability of LFAC System
HVAC Transmission System	1.463E-05		
HVDC Transmission System		3.599E-05	
LFAC Transmission System			3.831E-05
HVAC Transmission Line	4.888E-06		
HVDC Transmission Line		4.265E-06	
LFAC Transmission Line			3.208E-06
Wind Turbine (WT)	0.0032	0.0032	0.0032
Converter (AC/DC)		1.099E-05	1.092E-05
Large Converter (DC/AC)		1.099-05	1.099E-05
Cycloconverter			1.099E-05
20 Hz Interconnection Line			3.2084E-06
20 Hz Transformer			1.657E-07
Small Switch (SSW)	1.032E-05	1.032E-05	1.032E-05
Large Switch Failure	9.576E-06	9.582E-06	9.582E-06

(LSW)			
In Farm AC Transmission Line (FAC)	8.359E-06	8.359E-06	
In Farm DC (IFDC) Transmission Line			4.890E-06
Large Transformer (LT)	1.657E-07	1.656E-07	1.970E-07
Small Transformer (ST)	1.823E-07	2.304E-07	1.824E-07
AC Bus	1.198E-10		
DC Bus		1.198E-10	1.198E-10

The results in Table 15 demonstrate that the wind turbines have the maximum failure probability of 0.003177, and the AC and DC buses have the minimum failure probability of 1.197810e-010. The failure probability of HVAC transmission system is the lowest among the three transmission systems: 1.463E-05 for HVAC, 3.599E-05 for HVDC, and 3.831E-05 for LFAC, respectively.

8 ENHANCING TRANSMISSION SYSTEM RELIABILITY USING GENERATION PREDICTION TOOLS

8.1 Wind Power Generation Prediction

Since large-scale storage of offshore electricity is not feasible, efficient and effective forecasting, or prediction, models of offshore wind resource availability for smooth power production planning is critical. If the offshore wind power transmission operators can predict the wind power generation more efficiently and reliably using the forecasting tools, they can initiate proactive plans to enhance the transmission systems reliability. In this section of this thesis regression and machine learning-based wind resource prediction methods to forecast one, two, and seven days of wind power generation potentials of the US East and West Coasts are presented and discussed. Specifically, the forecasting methods that are presented and discussed in some details are: Auto Regressive Integrated Moving Average (ARIMA), Random Forest (RF), Bagging Classification and Regression Trees (BCART), and two hybrid models of ARIMA-RF and ARIMA-BCART.

8.1.1 Single-Stage Forecasting Models

Details of the single-stage forecasting methods are presented below.

8.1.1.1 Non-Seasonal ARIMA Model

ARIMA is one of the most sought-after stochastic models for analyzing time-series data and predicting wind power generation. ARIMA comprises different types of time series, such as pure autoregressive (AR), integrated (I), pure moving average (MA), and combined AR and MA (ARMA) models [60], [61]. Once the time-series data is stationary, the autoregressive steps activate and determine the forecast value compared to the present value [61]. An autoregressive model of order p, abbreviated AR (p), is given by eq. (47) [61], [62].

$$y_t = \emptyset_1 y_{t-1} + \emptyset_2 y_{t-2} + \cdots . + \emptyset_p y_{t-p} + \in_t \tag{47}$$

Where y_t is stationary and represents power generation at time t, and $\emptyset_1$, $\emptyset_2$, …., $\emptyset_p$ are regression coefficients ($\emptyset_p \neq 0$). $\in_t$ is the error term. The moving average model of order q or the MA (q) model is defined as eq. (48) [62].

$$y_t = \in_t + \theta_1 \in_{t-1} + \theta_2 \in_{t-2} + \cdots . + \theta_q \in_{t-q} \quad (48)$$

If, p and q parameters are known as the AR and MA orders, respectively, the generalization of the ARMA model is represented by eq. (49) [62].

$$y_t = \alpha + \emptyset_1 y_{t-1} + \emptyset_2 y_{t-2} + \cdots . + \emptyset_p y_{t-p} + \in_t + \theta_1 \in_{t-1} + \theta_2 \in_{t-2} + \cdots . + \theta_q \in_{t-q} \quad (49)$$

The ARIMA(p, d, q) is illustrated by eq. (50) [62]

$$\phi(B)(1-B)^d y_t = \theta(B)\epsilon_t \quad (50)$$

where, $\nabla^d y_t = (1-B)^d y_t$ is ARMA(p, q) and B is the backshift operator.

8.1.1.2 Seasonal ARIMA Model

The regular periodic patterns in the time series are known as seasonality, denoted by parameter S. The ARIMA method has been used extensively to predict seasonal time series. The multiplicative seasonal ARIMA model is given as [60]:

$$\text{ARIMA } (p, d, q)*(P, D, Q)S \quad (51)$$

Where:

p = order of non-seasonal AR terms,

P = order of seasonal AR terms,

q = order of non-seasonal MA terms,

Q = order of seasonal MA terms,

d = order of non-seasonal differencing,

D = order of seasonal differencing, and

S = span of seasonality pattern.

The multiplicative seasonal ARIMA, or SARIMA, model is expressed by eq. (52) [62].

$$\Phi_P(B^s)\phi(B)\nabla_s^D\nabla^d y_t = \delta + \Theta_Q(B^s)\theta(B)\epsilon_t \quad (52)$$

Where ϵ_t is the error term,

$\Phi_P(B^s) = (1 - \Phi_1 B^s - \Phi_2 B^{2s} - \cdots - \Phi_P B^{Ps})$,

$\Theta_Q(B^s) = (1 + \Theta_1 B + \Theta_2 B^{2s} \ldots + \Theta_Q B^{Qs})$,

$\phi(B) = 1 - \emptyset_1 B - \emptyset_2 B^2 \ldots - \emptyset_P B^p$,

$\theta(B) = 1 + \theta_1 B + \theta_1 B^2 + \cdots + \theta_Q B^q)$,

$\nabla^d = (1 - B)^d$, $\nabla_s^D = (1 - B^s)^D$.

The more detailed equation is denoted with eq. (53) [62].

$$(1 - \emptyset_1 B - \emptyset_2 B^2 - \cdots . - \emptyset_P B^p)(1 - \Phi_1 B^s - \Phi_2 B^{2s} - \cdots - \Phi_P B^{Ps})\ (1 - B^s)^D (1 - B)^d y_t = \left(1 + \theta_1 B + \theta_1 B^2 + \cdots + \theta_Q B^q)\right)(1 + \Theta_1 B + \Theta_2 B^{2s} + \cdots + \Theta_Q B^{Qs})\epsilon_t \quad (53)$$

The non-seasonal AR and MA parts are denoted by $\phi(B)$ and $\theta(B)$ with orders p and q, respectively, and the seasonal AR and MA parts are denoted by $\Phi_P(B^s)$ and $\theta_Q(B^s)$ of orders *P* and *Q*.

8.1.1.3 Random Forest Model

A decision tree was presented by Breiman in 1984 and Random Forest, the generalization of decision trees, was presented by Breiman in 2001 [63], [64], [65]. This method aggregates tress and is used for the classification or regression to avoid overfitting. Among the tree predictors, the most important tree is voted for in the forest and among the large number of trees [65]. The error for forests becomes low if the number of trees is large. This method can handle a vast number of features and assist in choosing features based on significance. This model is user friendly and only uses two free parameters of bootstrapping ensembles n_{trees} (default 500), where n is the number of trees, and the randomized input predictors sample is m_{try} (default 2) [64].

Random Forest (RF) has an ensemble of B trees $\{T_1(X), \dots, T_B(X)\}$, where $X = \{x_1, \dots, x_p\}$ is a p-dimensional vector of explanatory variables. The ensemble generates B outputs $\{\hat{Y}_1 = T_1(X), \dots, \hat{Y}_B = T_B(X)\}$,where $\hat{Y}_b = 1, \dots, B$, is the prediction of the bth tree [69]. The final prediction is the average of the individual tree prediction, $\hat{Y}$ [65], [66], [67]. The training method involves constructing a predictor, h(X), where the characteristics are recursively divided into nodes with distinct levels, Y. The RF, ensemble-based approach only emphasizes the ensemble of decision trees and gives this machine learning approach flexibility and computing power [60]. This requirement is not possible when children nodes with different labels exist. The terminal nodes are referred to as tree leaves and display the various possible labels of Y [65]. If the tree predictor of a random forest is h(X) and the distribution of vector Y, X, the mean-squared error for any numerical predictor is as follows [66].

$$E_{X,Y}\big(Y - h(X)\big)^2$$

8.1.1.4 Bagging Classification and Regression Trees (BCART)

Bootstrap Aggregating (bagging) is a widely used technique to combine many predictors to create a precise technique, introduced in 1994 by Leo Breiman [68]. This technique uses the bootstrap replication method to train the original data set, and a predictor is produced for each replicate sample. The predictors are combined using the average function for regression, and the majority vote for classification [68]. Here, a learning set is given by $\mathcal{L} = \{(y_n, x_n), n = 1, \dots., N\}$, where, y is the class level, or a result, for an input x, and the output predictor, y, is denoted by $\varphi(x, \mathcal{L})$. If the output y is the numerical response, the average function of the predictor proposed by Breiman is given by eq. (54) [68], [69].

$$\varphi_B(x) = av_B\varphi\big(a, \mathcal{L}^{(k)}\big) \tag{54}$$

8.1.1.4.1 Bagging Classification Trees

The data set is organized indiscriminately into a test set T and learning set $\mathcal{L}$. In most cases, the learning set $\mathcal{L}$ would be reasonably large [69]. The 10-fold cross-validation builds a classification tree from $\mathcal{L}$. This tree generates the miscalculation rate $e_s(\mathcal{L}, \mathrm{T})$. Using the10-fold cross-validation, a tree is built using a bootstrap sample, $\mathcal{L}_B$.

The tree classifiers will be $\varphi_1(x), \varphi_2(x), \ldots\ldots, \varphi_{50}(x)$, if it repeats 50 times. If $(j_n, x_n)(x) \in$ T, then x_n has the plurality of $\varphi_1(x_n), \varphi_2(x_n), \ldots\ldots, \varphi_{50}(x_n)$. If the estimated class differs from the original, the bagging miscalculation rate is $e_B(\mathcal{L}, \mathrm{T})$.

8.1.1.4.2 Bagging Regression Trees

The data set is processed spontaneously into a test set T and learning set $\mathcal{L}$. Normally, an $\mathcal{L}$ of 200 cases is generated for the learning set, and 1,000 cases are generated for the test set. By 10-fold cross-validation, a regression tree is built from $\mathcal{L}$. The tree creates the mean-squared-error $e_s(\mathcal{L}, \mathrm{T})$ [69]. A regression tree is built using a bootstrap replicate $\mathcal{L}_B$. The predictor will be $\varphi_1(x), \varphi_2(x), \ldots\ldots, \varphi_{25}(x)$, if it repeats 50 times. If $(y_n, x_n)(x) \in$ T, the predicted $\hat{y}_B$ value will be $av_k\varphi_k(x_n)$. The mean-squared-error is $e_B(\mathcal{L}, \mathrm{T})$ in T. The single tree and bagged error over 100 iterations are $\overline{e}_s$ and $\overline{e}_B$.

8.1.2 Hybrid Model

8.1.2.1 Background of Hybrid Model

Real-world time series data are rarely purely linear or non-linear, although both linear and non-linear data are typically used. The ARIMA model alone is not sufficient for non-linear data management, while machine learning models are not equally capable of managing both linear and non-linear data [61]; therefore, no single approach is appropriate [61], [70]. The Monte Carlo simulation, or bootstrapping method, has been popularized to forecast non-

linear patterns because the distribution of the error mechanism does not require any assumptions [71]. The machine learning RF model uses bootstrap sampling, and the bootstrap replication method is used in the BCART model. Compared to a single process, the hybrid method performs well [73]. We can capture various aspects of the underlying trends of time series results by integrating differences and can capture the underlying patterns of time series data by combining different models. If we assume that a time-series data set consists of a linear autocorrelation structure and a non-linear component, the data should be expressed as follows [61].

$$y_t = L_t + N_t \tag{55}$$

Where the linear component is denoted by L_t and the non-linear component is denoted by N_t. For the linear component, we use ARIMA and then determine the residuals from the linear component that contains a non-linear relationship. The residual from the linear model at time t is expressed as follows.

$$r_t = y_t - \widehat{L_t} \tag{56}$$

Here, $\widehat{L_t}$ is the forecast value with time t.

By modeling residuals using the bootstrap sampling method in RF and the bootstrap replication method in BCART, the non-linear forecast value $\widehat{N_t}$ can be found. Then, the combined forecasted value, $\hat{y}_t$will be as follows.

$$\hat{y}_t = \widehat{L_t} + \widehat{N_t} \tag{57}$$

8.1.2.2 ARIMA-RF

The predictor variables are used to train the ARIMA model in the first step. If the relationship between wind power generation and the atmospheric variables is non-linear, ARIMA will not capture the non-linear component of the data; however, the ARIMA model's residual will contain non-linear information. The residuals from the ARIMA model are used to analyze the non-linear structure of the data in the second step, after which we combine the

forecasts to improve the overall performance. If the forecasted value in the first step is $\hat{F}$ and the calculated forecasted value from the second step is $\hat{R}$, the final forecasted value, $\hat{y}_t$will be

$$\hat{Y} = \hat{F} + \hat{R} \tag{58}$$

The RF model based on ensemble-based method emphasizes only on ensembles of decision trees [60]. It is extremely effective in handling large datasets because it uses a small random portion of the dataset, and it performs better over other machine learning approach. Therefore, the performance of ARIMA-RF model is better than other hybrid combinations [61].

The flowchart of the two-stage hybrid model is displayed in Fig. 29 [61].

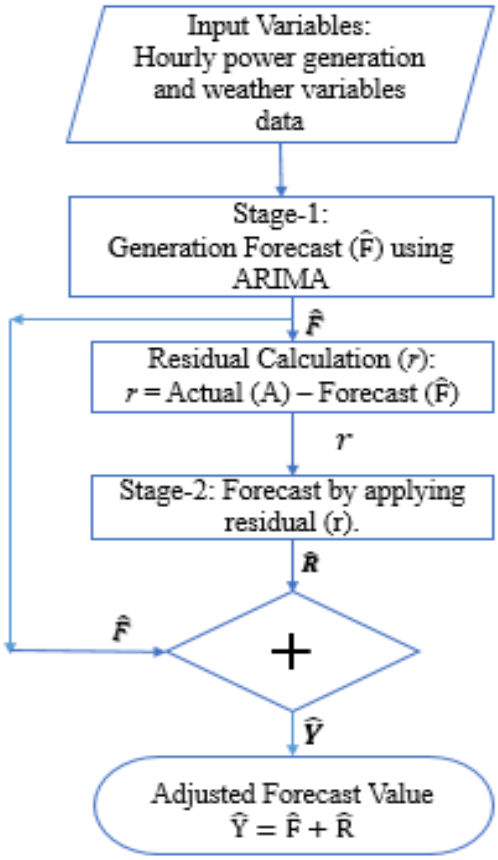

Fig. 29. The flowchart of the two-stage ARIMA-RF hybrid model [60].

8.1.2.3. ARIMA-BCART

The initial stage is similar to the previous model. The residuals from the ARIMA model are fed to the BCART model to predict the forecasted value from the residuals. If the forecasted value in the first step is $\hat{F}$ and the calculated forecasted value from the second step is $\hat{R}$, the final forecasted value $\hat{y}_t$ will be as follows.

$$\hat{Y} = \hat{F} + \hat{R} \tag{59}$$

8.2 Forecasting Methodology

This thesis has used the National Renewable Energy Laboratory (NREL) wind toolkit for 2009-2012, which contains estimated wind power generation data from four different sites along the US east and west coasts. The training datasets contain wind turbine power data and weather data such as wind speed, wind direction, air temperature, surface air pressure, and air density at hub height [74]. The models are used to predict wind power for three different durations: 24 hours, 48 hours, and 7 days. The performance of these models has been analyzed by using two commonly used statistical indices, Normalized Mean Absolute Error (NMAE) and Normalized Root Mean Square Error (NRMSE). MAE and RMSE errors are expressed by eqs. (60) and (61), respectively. Their normalized expressions are given by eqs. (62) and (63), respectively.

$$MAE = \frac{\sum_{i=1}^{N} |P_{ai} - P_{fi}|}{N} \tag{60}$$

$$RMSE = \sqrt{\frac{1}{N}\sum_{i=1}^{N}(P_{ai} - P_{fi})^2} \tag{61}$$

where P_{ai} and P_{fi}, respectively, signify the actual and forecasting value of wind power output at time I, and N is the number of forecast samples involved.

$$NMAE = \frac{MAE}{Mean\ of\ the\ Generation\ Data} \times 100\% \tag{62}$$

$$NRMSE = \frac{RMSE}{Mean\ of\ the\ Generation\ Data} \times 100\% \quad (63)$$

This thesis has used the Spearman correlation method to determine the significant features for each site. Input variables are ranked based on their correlation co-efficient.

Table 16. Spearman Correlation Coefficient of Input Variables to Wind Power Generation.

Explanatory variables	East Coast-1	East Coast-2	West Coast-1	West Coast-2
Wind speed at 100m height	0.922	0.920	0.85	0.844
Wind direction at 100m height	0.102	0.102	-0.30	-0.288
Air temperature at 2m	-0.174	-0.175	0.16	0.147
Surface air pressure	-0.304	-0.302	-0.10	-0.099
Air density	0.045	0.045	-0.11	-0.099

The data in Table 16 illustrates that the three significant weather variables from the East coast data sets are different from the West coast data sets. Wind speed is the most important feature, while wind direction and air temperature are the next two important variables for the west coast sites, and surface air pressure and air temperature are the most important variables for the east coast sites. Insignificant variables can be removed from the training datasets, as their contribution will be minimal for wind power generation prediction. This thesis has also compared the performance of the algorithms based on these three most important variables.

8.3. Forecasting Result and Discussion

The single-stage method of ARIMA, RF and BCART, and the two-stage hybrid models of ARIMA-RF and RIMA-BCART have been used to predict wind power generation from

the US East and West coast windfarms. The models are analyzed using the datasets with durations of 24 hours, 48 hours, and 7 days. We have evaluated the accuracy of the forecasted models with the statistical indices of NMAE and NRMSE.

The comparison of the performance in terms of NMAE with the different datasets from the US East and West coasts with five weather variables (wind speed, wind direction, air temperature, air pressure, and air density at hub height) are shown in Table 17 and Fig. 30, and the three significant weather variables (wind speed, air temperature and surface air pressure for east coast and wind speed, wind direction and air temperature for west coast) are shown in Table 18 and Fig. 31.

Table 17. Comparison of NMAE for five weather variables data (wind speed, wind direction, air temperature, air pressure, and air density at hub height).

Time	Location	ARIMA	RF	BCART	ARIMA-RF	ARIMA-BCART
24H	Eastcoast-1	33.63%	0.52%	6.60%	26.52%	26.75%
	Eastcoast-2	33.46%	0.53%	6.56%	30.05%	29.96%
	Westcoast-1	24.29%	0.27%	5.50%	20.70%	21.76%
	Westcoast-2	18.32%	0.19%	4.89%	16.60%	16.47%
48H	Eastcoast-1	33.42%	0.98%	8.20%	27.12%	27.25%
	Eastcoast-2	33.10%	1.29%	9.23%	27.19%	28.34%
	Westcoast-1	26.11%	0.32%	6.05%	22.05%	22.77%
	Westcoast-2	20.33%	0.23%	6.02%	17.47%	17.23%
7 DAYS	Eastcoast-1	29.82%	1.79%	9.49%	24.02%	24.27%
	Eastcoast-2	30.23%	2.18%	9.54%	24.90%	26.81%
	Westcoast-1	38.23%	4.03%	12.19%	31.80%	34.26%

	Westcoast-2	40.46%	3.40%	13.71%	33.59%	35.35%

Table 18. Comparison of NMAE for three significant weather variables (wind speed, air temperature and surface air pressure for east coast and wind speed, wind direction and air temperature for west coast).

Time	Location	ARIMA	RF	BCART	ARIMA-RF	ARIMA-BCART
24H	Eastcoast-1	33.40%	0.50%	7.56%	29.71%	28.71%
	Eastcoast-2	31.40%	0.49%	7.35%	27.26%	27.15%
	Westcoast-1	18.10%	0.37%	5.98%	15.54%	17.23%
	Westcoast-2	18.32%	0.37%	6.12%	16.60%	16.85%
48H	Eastcoast-1	33.36%	0.96%	9.41%	28.13%	26.92%
	Eastcoast-2	32.38%	0.85%	9.31%	27.56%	28.37%
	Westcoast-1	18.50%	0.37%	6.47%	15.82%	17.81%
	Westcoast-2	19.79%	0.37%	6.68%	16.26%	16.97%
7 DAYS	Eastcoast-1	29.97%	1.24%	10.87%	24.03%	26.11%
	Eastcoast-2	29.78%	0.93%	10.66%	24.18%	25.31%
	Westcoast-1	35.24%	5.86%	14.61%	29.20%	30.47%
	Westcoast-2	34.08%	5.51%	14.91%	15.87%	16.47%

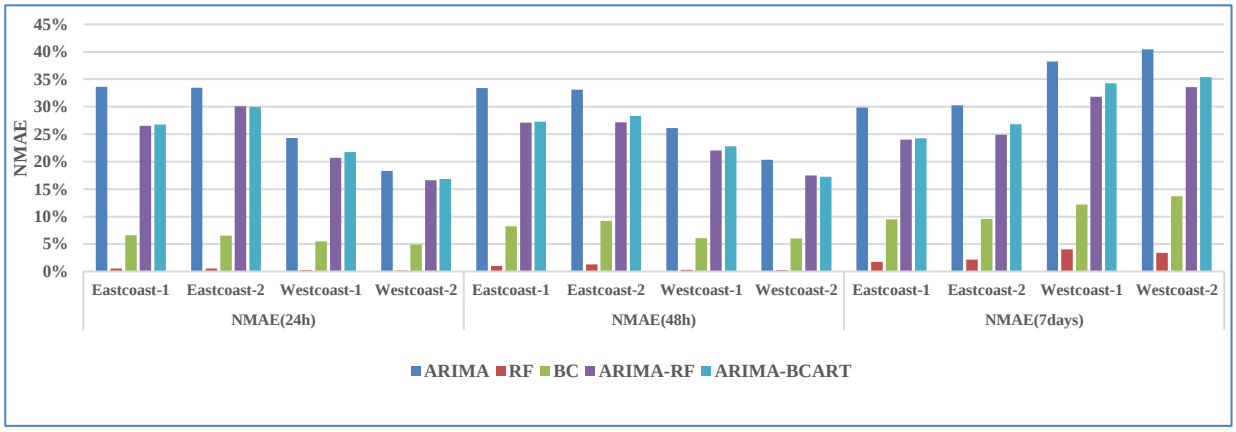

Fig. 30. Comparison of NMAE with different data sets containing five weather variables (wind speed, wind direction, air temperature, air pressure, and air density at hub height).

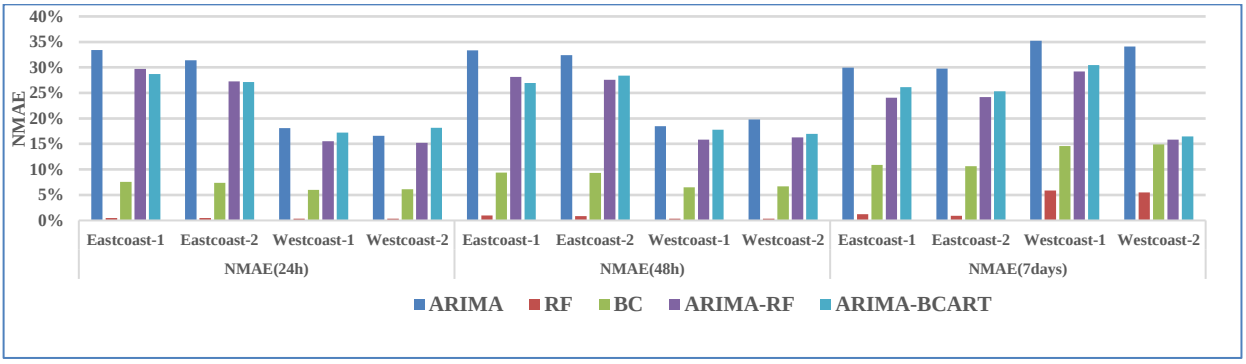

Fig. 31. Comparison of NMAE with different data sets containing three significant weather variables (wind speed, air temperature and surface air pressure for east coast and wind speed, wind direction and air temperature for west coast).

Table 17 and Fig. 30 show RF model has better prediction rates for all time durations. Since, the relationship between the output and predictor variables are non-linear, and ARIMA is not suited for modeling non-linear data, the performance of ARIMA is the least among all methods; however, RF and BCART have greater prediction accuracy in terms of NMAE. To

improve the accuracy of ARIMA, the hybrid models are introduced where the residuals of ARIMA are passed to both RF and BCART machine learning algorithms. ARIMA-RF and ARIMA-BCART models reveal a significant improvement in prediction. ARIMA-RF has reduced the error rate by 13% - 17% for different prediction period. ARIMA-BCART has slightly less accuracy than ARIMA-RF and improved the average accuracy by 10%-15%. The Table 18 and Fig. 31 show that the accuracy has slightly increased for the three important variables (wind speed, air temperature and surface air pressure for east coast and wind speed, wind direction and air temperature for west coast).

For different prediction intervals, ARIMA-RF has reduced the error rate by 13% - 27%. ARIMA-BCART is marginally less robust than ARIMA-RF and has minimized the error rate by 10%-23% on average. The comparison of the prediction accuracy in terms of NRMSE for the US East and West coast datasets with five weather variables are recorded in Table 18 and Fig. 32, and the three significant weather variables according to spearman correlation are shown in Table 18 and Fig. 33.

Table 19. Comparison of NRMSE for five weather variable data.

Time	Location	ARIMA	RF	BCART	ARIMA-RF	ARIMA-BCART
24H	Eastcoast-1	40.58%	0.61%	7.69%	31.17%	32.55%
	Eastcoast-2	41.37%	0.67%	7.07%	35.09%	35.70%
	Westcoast-1	28.26%	0.27%	6.58%	24.10%	25.33%
	Westcoast-2	38.62%	0.63%	6.60%	19.03%	18.79%
48H	Eastcoast-1	39.67%	2.63%	9.15%	32.74%	35.34%
	Eastcoast-2	39.83%	3.37%	11.02%	33.73%	34.43%
	Westcoast-1	29.13%	0.32%	6.80%	25.36%	25.55%
	Westcoast-2	37.18%	3.14%	10.29%	20.11%	19.94%

7 DAYS	Eastcoast-1	48.16%	4.95%	22.62%	38.15%	45.07%
	Eastcoast-2	48.59%	6.06%	22.68%	39.38%	45.44%
	Westcoast-1	64.43%	4.03%	31.78%	53.90%	60.72%
	Westcoast-2	67.13%	5.65%	21.18%	55.24%	59.25%

Table 20. Comparison of NRMSE for three most important variables

Time	Location	ARIMA	RF	BCART	ARIMA-RF	ARIMA-BCART
24H	Eastcoast-1	40.08%	0.60%	8.63%	34.48%	34.52%
	Eastcoast-2	36.96%	0.58%	8.59%	31.84%	32.13%
	Westcoast-1	21.19%	0.44%	7.20%	17.72%	20.05%
	Westcoast-2	23.38%	0.45%	7.29%	20.13%	20.26%
48H	Eastcoast-1	39.63%	2.21%	10.35%	32.88%	34.82%
	Eastcoast-2	37.87%	2.12%	10.35%	32.25%	34.22%
	Westcoast-1	21.14%	0.45%	7.40%	17.81%	19.39%
	Westcoast-2	22.07%	0.45%	7.55%	17.80%	18.48%
7 DAYS	Eastcoast-1	48.11%	3.58%	21.94%	38.02%	44.68%
	Eastcoast-2	49.23%	2.58%	21.90%	38.67%	44.88%
	Westcoast-1	65.90%	27.98%	39.06%	55.58%	57.98%
	Westcoast-2	63.99%	26.31%	39.07%	17.34%	17.69%

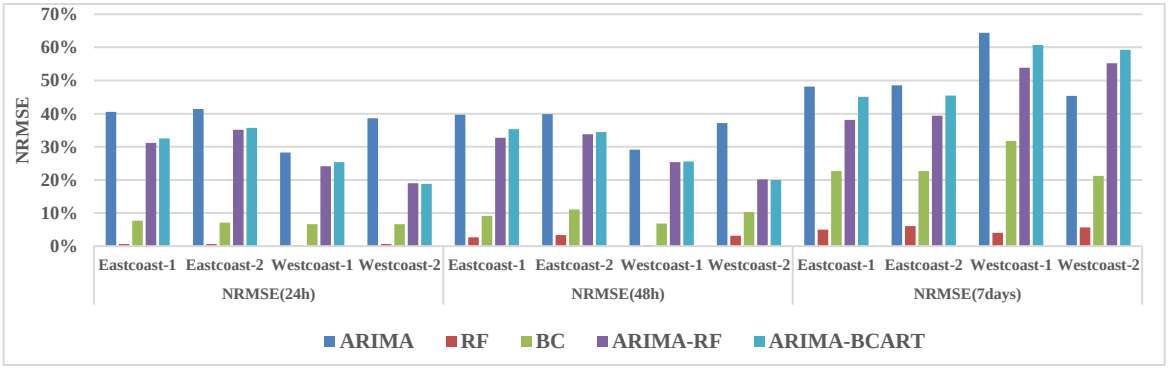

Fig. 32. Comparison of NRMSE of different datasets with five weather variables

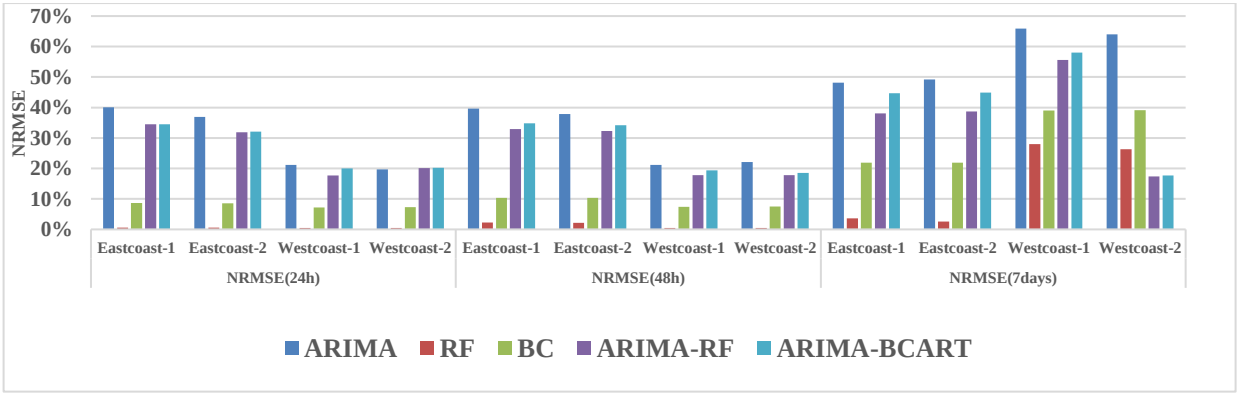

Fig. 33. Comparison of NRMSE of different datasets with three significant weather variables.

The results of NRMSE in Table 19 and 20 are as similar as the NMAE. Both ARIMA-RF and ARIMA-BCART have significantly improved the accuracy with five weather variables. ARIMA-RF has decreased the error rate by 18% - 26% for different prediction periods. ARIMA-BCART is marginally less powerful than ARIMA-RF and has increased the average accuracy by 8%-24%. Similar enhancements are noticeable for forecasting using three crucial weather parameters, and the ARIMA-RF and ARIMA-BCART have boosted the prediction accuracy by 15%-32% and by 12%-24%, respectively.

8.4 Conclusion of Forecasting

The prediction of wind power generation is vital for offshore power transmission system operators to boost their transmission system reliability. This research has identified that the error rate in ARIMA is relatively high. This thesis has shown the two-stage hybrid methods have improved the prediction accuracy of ARIMA. The results have demonstrated that hybrid models are best suitable for time series data, where both linear and non-linear features are present. The performance of both ARIMA-RF and ARIMA-BCART models are similar for wind power prediction, but the performance of ARIMA-RF model is slightly better than ARIMA-BCART model. Since, the RF model uses the ensemble-based method which emphasizes only on ensembles of decision trees, and it uses a small random portion of dataset for learning, the ARIMA-RF model performs better over other hybrid combinations. The proposed hybrid models have boosted ARIMA's performance by 8% -26% on average. This efficient and reliable forecasting tool can be successfully used to enhance the offshore transmission system reliability.

9 CONCLUSSION AND FUTURE WORK

9.1 Conclusion

This thesis has investigated the HVAC, HVDC, and LFAC transmission topologies of offshore wind power plants and their reliability performance. The thesis has also briefly explained the advantages of the LFAC transmission system compared to the other two transmission systems. The reliability performance of the three transmission systems has been studied using the FTA method. The thesis work can be summarized into five contributions. Contribution 1 is to explore three transmission topologies, and to highlight the efficiency and cost-effectiveness of the LFAC transmission system. Contribution 2 is to discuss the history and introduction of the FTA method into the power system industry. Contribution 3 is to build the state of the art simulation model of the three transmission systems. Contribution 4 is to analyze the reliability performance of the three transmision systems, and Contribution 5 is to present the efficient and reliable offshore wind power generation forecasting tools to enhance transmission system's reliability.

The key findings of this research are as follows:

1. The simulation models identified the minimal cut sets and failure probabilities of the three transmission systems. The thesis has also determined the time-based reliability indices such as mean unavailability and number of failures of the systems at 10,000 hours, the CIM, and the RRW of the three transmission system components.
2. The major fault event was generated from wind turbines for all the three transmission systems, and the large switch is the most critical piece of equipment for the HVAC system; AC/DC and DC/AC converter is the most critical piece of equipment in the HVDC system, and DC/AC converter is a most critical component of the LFAC transmission system.

3. The AC bus has the lowest risk reduction, and the large switch has the highest risk reduction in the HVAC transmission system. The DC bus has the lowest risk reduction, and AC/DC and DC/AC converters have the highest risk reductions in the HVDC transmission system. The DC bus has the lowest risk reduction and DC/AC converter and Cycloconverter have the highest risk reductions in the LFAC transmission system.
4. The transmission system failure probability of HVAC is the lowest among the three transmission systems: 1.463E-05, 3.599E-05, and 3.831E-05, respectively.
5. In contribution 5, hybrid forecasting approaches using ARIMA, RF and BCART models were explored. The preliminary results indicate that ARIMA-RF and ARIMA-BCART models perform better over standalone ARIMA to predict wind power production.

9.2 Future Work

The Monte Carlo simulation and Markov chain methods can be used to further analyze the reliability performnace of the offshore windfarm transmission system topologies. Future work can also investigate and evaluate the feasibility of Failure Mode and Effect Analysis (FMEA) of the offshore wind power transmission topplogies to enhance their respective systems' reliabilty.

PUBLICATIONS BASE ON THIS RESEARCH WORK:

Ashoke Kumar Biswas, Shravan Kumar Akula, Sina Ibne Ahmed, Hossein Salehfar, "*Low-Frequency AC Transmission Topology and Reliability Analysis*", The 52nd North American Power Symposium (NAPS) 2021.

Ashoke Kumar Biswas, Sina Ibne Ahmed, Shravan Kumar Akula, Hossein Salehfar, "*High Voltage AC (HVAC) and High Voltage DC (HVDC) Transmission Topologies of Offshore Wind Power and Reliability Analysis*", IEEE GreenTech Conference 2021.

Ashoke Kumar Biswas, Sina Ibne Ahmed, Temitope Bankefa, Prakash Ranganathan, Hossein Salehfar, "*Performance Analysis of Short and Mid-Term Wind Power Prediction using ARIMA and Hybrid Models*", IEEE Power and Energy Conference at Illinois (PECI) 2021.

REFERENCES

[1] X. Xiang, M. M. C. Merlin, and T. C. Green, "Cost Analysis and Comparison of HVAC, LFAC and HVDC for Offshore Wind Power Connection," 12th IET International Conference on AC and DC Power Transmission (ACDC 2016), Beijing, 2016, pp. 1-6, doi: 10.1049/cp.2016.0386.

[2] G. F. Reed, H. A. Al Hassan, M. J. Korytowski, P. T. Lewis, and B. M. Grainger, "Comparison of HVAC and HVDC Solutions for Offshore Wind Farms with a Procedure for System Economic Evaluation," 2013 IEEE Energytech, Cleveland, OH, 2013, pp. 1-7, doi: 10.1109/EnergyTech.2013.6645302.

[3] A. S. Dobakhshari and M. Fotuhi-Firuzabad, "A Reliability Model of Large Wind Farms for Power System Adequacy Studies," IEEE Transactions on Energy Conversion, September 2009, vol. 24, no. 3, pp. 792-801, doi: 10.1109/TEC.2009.2025332.

[4] C. Monteiro, R, Bessa, V., Miranda, A. Botterud, J. Wang, Jianhui, G. Conzelmann, G., Sciences, Decision, & Porto, INESC, Wind Power Forecasting: State-of-the-Art, Argonne National Laboratory, 2009.

[5] N. Sabrina, A. Sharif, R. Vishwajit, B. Stephen, Analysis and Application of Seasonal ARIMA Model in Energy Demand Forecasting: A Case Study of Small Scale Agricultural Load, Department of Electrical and Computer Engineering, Texas Tech University.

[6] U.S. Department of Energy (DOE), 20% Wind Energy by 2030: Increasing Wind Energy's Contribution to U.S. Electricity Supply, DOE Office of Energy Efficiency and Renewable Energy Report, July 2008. http://www1.eere.energy.gov/windandhydro/wind_2030.html.

[7] Chaithanya, S. & Reddy, Naga Bhaskar & Kiranmayi, R. (2018) " A state of the art review on offshore wind power transmission using low-frequency AC system", International Journal of Renewable Energy Research. 8. 141-149.

[8] Xu L and B. R. Andersen, "Grid Connection of Large Offshore Wind Farms Using HVDC," Wind Energy, 2006, vol. 9, pp. 371–382.

[9] F. Martinez-Rodrigo, D. Ramirez, H. Mendonça, and S. de Pablo, "MMC as Nonlinear Vector Current Source for Grid Connection of Wave Energy Generation," International Journal of Electrical Power & Energy Systems, 2019, vol. 113, pp. 686-698.

[10] Power Systems Engineering Research Center "Low-Frequency Transmission", PSERC Publication 12- 28, October 2012.

[11] Xifan Wang and Xiuli Wang, "Feasibility study of fractional frequency transmission system," in IEEE Transactions on Power Systems, vol. 11, no. 2, pp. 962-967, May 1996, doi: 10.1109/59.496181.

[12] C. C. Fong, et al., "Bulk System Reliability - Measurement and Indices," IEEE Trans. Power Systems, August 1989, vol. 4, no. 3, pp. 829-835.

[13] Baig Ahmed Ali, Ruzli Risza, and Buang Azizul B., "Reliability Analysis Using fault tree analysis: A reriew", International Journal of Chemical Engineering, Vol. 4, No. 3, June 2013.

[14] Olimpo Anaya-Lara et al, "Wind Energy Generation Modeling and Control", 1st ed. Chichester, U.K.: Wiley, 2009.

[15] Madariaga A, de Alegria IM, Martín JL, Eguía P, Ceballos S. "Current facts about offshore wind farms". Renewable Sustain Energy Rev 2012; 16: 3105–16.

[16] J. Dakic, M. Cheah-Mane, O. Gomis-Bellmunt, and E. Prieto Araujo, "HVAC Transmission System for Offshore Wind Power Plants Including Mid-cable Reactive Power Compensation: Optimal Design and Comparison to VSC-HVDC Transmission," IEEE Transactions on Power Delivery, doi: 10.1109/TPWRD.2020.3027356.

[17] I. Martínez de Alegría, J. L. Martín, I. Kortabarria, J. Andreu, and P. I. Ereño, "Transmission Alternatives for Offshore Electrical Power," Renewable and Sustainable Energy Reviews, 2009, vol. 13, no. 5, pp. 1027-1038.

[18] W. Kling, et al., "Advanced Transmission Solutions for Offshore Wind Farms: Power and Energy Society General Meeting-Conversion and Delivery of Electrical Energy in The 21st Century," IEEE, 2008, pp. 1-6.

[19] Warnock, J.; McMillan, D.; Pilgrim, J.; Shenton, S. "Failure Rates of Offshore Wind Transmission Systems". *Energies* 2019, *12*, 2682.

[20] R. Chokhawala, B. Danielsson, and L. Angquist, "Power Semiconductors in Transmission and Distribution Applications," Proceedings of the 13th International Symposium on Power Semiconductor Devices & ICs, 2001, pp. 3-10 IPSD '01 (IEEE Cat. No.01CH37216), Osaka, Japan, doi: 10.1109/ISPSD.2001.934548

[21] R T. Volker, C. Mehler, H. Raffel, and B. Orlik, "New HVDC-Concept for Power Transmission from Offshore Wind Farms," Wind Power to the Grid—EPE Wind Energy Chapter 1st Seminar, Delft, The Netherlands, March 2008; pp. 1-6.

[22] A. Jos, “High Voltage Direct Current Transmission,” Second Edition, Institution of Electrical Engineers, 1998, ch. 7, pp. 159-199. ISBN 0-85296-941-4.

[23] J. Tianyi, "Internal Fault Diagnosis of MMC-HVDC Based on Classification Algorithms in Machine Learning," Theses and Dissertations, 2089, 2019, https://dc.uwm.edu/etd/2082.

[24] J. Todorovic, “Losses Evaluation of HVAC Connection of Large Offshore Wind Farms,” Masters Thesis, Royal Institute of Technology, Department of Electrical Engineering, Stockholm, Sweden, 2004.

[25] R. Ryndzionek, L. Sienkiewicz, “Evolution of the HVDC Link Connecting Offshore Wind Farms to Onshore Power Systems,” Energies, Published April 14, 2020.

[26] Fischer W, Braun R, Erlich I. “Low frequency high voltage offshore grid for transmission of renewable power” In: Proceedings of the 2012 3rd IEEE PES innovative smart grid technologies Europe, 2012.

[27] Pfeiffer A, Scheidl W, Eitzmann M, Larsen E. “Modern rotary converters for railway applications”. In: Proceedings of the 1997 IEEE/ASME joint railroad conference, 1997. p. 29–33.

[28] Frey S. Railway electrification systems and engineering. Delhi: White Word Publications; 2012.

[29] X. wang, “The Fractional Frequency Transmission System”, in 1994 IEE Japan Power & Energy, pp. 53-58.

[30] Mazahar. H, Jie. Wang, and Gulam. S. Kaloi, “A Review of the State of the Art Control Techniques for Wind Energy Conversion System", International Journal of Renewable Energy Research (IJRER), vol. 6, no. 4, pp. 12-76-1295, 2016.

[31] Marco Liserre, and Marta Molinas “Overview of Multi-MW wind turbines and wind parks”, IEEE Trans on Indus Elec : 2011;58 : pp. 1081-95.

[32] Song Z, Wang X, Xiao Y, Liu S. “PMSG-based fractional frequency wind power system”. In: Proceedings of the 2014 IEEE innovative smart grid technologies –Asia (ISGT Asia), 2014.

[33] Camara, M.S., Camara, M.B., Dakyo, B. and Gualous, H., “Permanent Magnet Synchronous Generator for Offshore Wind Energy System Connected to Grid and Battery-Modeling and Control Strategies”, International Journal of Renewable Energy Research (IJRER), vol. 5, no. 4, pp. 386-393,2015.

[34] Sekhar, K. Ramachandra, Rohan Barot, Prashant Patel, and N. Vinoth Kumar. "A novel topology for improved DC bus utilization in PMSG based wind energy generation system." In Renewable Energy Research and Applications (ICRERA), IEEE International Conference, pp. 525-530. 2015.

[35] P B Wylli, Y Tung, L Ran, T Yung, J Yu. “Low frequency AC transmission–Elements of a design for wind farm connection”. In: Proceedings of the 11th IET International Conference on AC and DC power transmission, 2015.

[36] Philips T. Krein, “Element of Power Electronics”, 1998

[37] Troyer Drew, “ Reliability Engineering Principles for the plant engineer, Noria Corporation, Available: https://www.reliableplant.com.

[38] Charles. E. Ebeling, “An Introduction to Reliability and Maintainability Engineering”, Third Edition.

[39] Schenkelberg, Carlson Carl S., “Introduction to R & M Management”, Available: https://www.webull.com.

[40] A. Birolini, Reliability Engineering, “Theory and Practice”, Fourth edition.

[41] R. Billinton and R. N. Allan, "Power-system reliability in perspective," in Electronics and Power, vol. 30, no. 3, pp.231-236, March1984, URL: http://ieeexplore.ieee.org

[42] S. H. Madaeni, R. Sioshansi and P. Denholm, "The capacity value of solar generation in the Western United States," 2012 IEEE Power and Energy Society General Meeting, San Diego, CA, 2012, pp. 1-8.

[43] Fussell, J.B. , "Synthetic Tree Model A Formal Methodology For Fault Tree Calculation," Aerojet Nuclear Corporation Company, National Reactor Testing station, Idaho Falls, Idaho, IN-83401, 1973.

[44] Hassl D.F.,”Advanced, 1965, Concept in Fault tree Analysis” System Safety Symposium

[45] Chatterjee P, 1974, Fault Tree Analysis: Reliability Theory and Systems Safety, PhD Thesis, University of California, Berkeley.Microfim.

[46] Dan M. S & Joseph T, 2007, Condition-based fault tree analysis (CBTA): A new method for improved fault tree analysis (FTA), reliability and safety calculations, Reliability Engineering and System Safety.

[47] John Lekan, Akinode. (2017). Algorithms for Reducing Cut Sets in Fault Tree Analysis. 6. 36-41. 10.17148/IJARCCE.2017.61207.

[48] Lee, W S, Grosz, D L., Tillman F A, Lie, C H, 1985, Fault Tree Analysis, Methods, and Applications –A review: IEEE Transactions on Reliability.

[49] Sinnamon R M, 1996, Binary Decision Diagram, PhD Thesis, Loughborough University, UK.

[50] W. Vesely et al., Fault Tree Handbook, NUREG-0492, Nuclear Regulatory Commission, 1981.

[51] M. Stamatelatos, W. Vesely, J.B. Dugan, J. Fragola, J. Minarick, and J. Railsback. Fault Tree Handbook with Aerospace Applications. NASA Office of Safety and Mission Assurance, 2002.

[52] Apostolakis, G., T. L. Chu, and R. H. Whitley. Methodology and application of probabilistic evaluation to thermal reactor safety. Final report. No. EPRI-NP-1443. California Univ., Los Angeles (USA). School of Engineering and Applied Science, 1980.

[53] Whitehouse, Gary E. "GERT, A Useful Technique for Analyzing Reliability Problems." Technometrics, vol. 12, no. 1, 1970, pp. 33–48. JSTOR, www.jstor.org/stable/1267349. Accessed 8 Feb. 2021.

[54] American National Standards Institute, IEEE Guide for General Principles of Reliability Analysis of Nuclear Power Generating Station Safety Systems, ANSI/IEEE Std 352™-1987 (R2010) (Revision of ANSI/IEEE Std 352-1975).

[55] W. Feller, An Introduction to Probability Theory and Its Applications, Vol. I,John Wiley and Sons, Inc., New York, 1957, 1968.

[56] Fussell, J.B. , "A review of fault Tree Analysis with Empasis on Limitations" Aerojet Nuclear Company, Idaho Falls, Idaho, IN-83401, 1973.

[57] American Nuclear Society, 1972 Annual Meeting, Las Vegas, Navada, 1972, Vol. 15.

[58] W.E. Vesely, " A Time Dependant Mthodology for Fault Tree Evaluation," Nucl. Eng. Design, 13, 337 (1970).

[59] Relyence Corporation, Greensburg, PA, USA, Available: https://www.relyence.com.

[60] N. Sabrina, A. Sharif, R. Vishwajit, B. Stephen, Analysis and Application of Seasonal ARIMA Model in Energy Demand Forecasting: A Case Study of Small Scale Agricultural Load, Department of Electrical and Computer Engineering, Texas Tech University.

[61] R. Angamuthu Chinnathambi, A. Mukherjee, M. Campion, H. Salehfar, T.M. Hansen, J. Lin, P.A. Ranganathan, Multi-Stage Price Forecasting Model for Day-Ahead Electricity Markets, Forecasting 2018, vol. 1, pp. 26-46, [pdf]. http://www.mdpi.com/2571-9394/1/1/3, 2018.

[62] G. P. Zhang, Time Series Forecasting Using a Hybrid ARIMA and Neural Network Model, Neurocomputing, Elsevier, vol. 50, pp. 159–175, 2003.

[63] R. Shumway and D. Stoffer, Time Series Analysis and Its Applications: With R Examples, ser. Springer Texts in Statistics, Springer New York, 2010.

[64] L. Breiman, Random Forests, Machine Learning, vol. 45, no. 1, pp. 5–32, 2001.

[65] A. Mumtaz, P. Ramendra, X. Yong, Y. Zaher undher, Complete Ensemble Empirical Mode Decomposition Hybridized with Random Forest and Kernel Ridge Regression Model For Monthly Rainfall Forecasts, Journal of Hydrology, vol. 584, 2020.

[66] A. Callens, D. Morichon, S. Abadie, M. Delpey, L. Benoit, Using Random Forest and Gradient Boosting Trees to Improve Wave Forecast at a Specific Location, Applied Ocean Research, vol. 104, 2020.

[67] A. Lahouar and J. Ben Hadj Slama, Random Forests Model for One Day Ahead Load Forecasting, IREC2015 The Sixth International Renewable Energy Congress, Sousse, 2015.

[68] Svetnik, V.; Liaw, A.; Tong, C.; Culberson, J. C.; Sheridan, R. P.; Feuston, B. P. Random Forest: A Classification and Regression Tool for Compound Classification and Qsar Modeling, J. Chem. Inf. Comp. Sci., vol. 43, pp. 1947−1958, 2003.

[69] S. Basterrech and V. Snášel, Time-series Forecasting Using Bagging Techniques and Reservoir Computing, International Conference on Soft Computing and Pattern Recognition (SoCPaR), Hanoi, pp. 146-151, 2013.

[70] L. Breiman, Bagging Predictors, Department of Statistics, University of California, Berkley, California 94720, USA, Tech. Rep. 421, September 1994.

[71] S. Makridakis, A. Anderson, R. Carbone, R. Fildes, M. Hibdon, R. Lewandowski, J. Newton, E. Parzen, R. Winkler, The Accuracy of Extrapolation (Time Series) Methods: Results of a Forecasting Competition, J. Forecasting 1,111–153, 1982.

[72] J. G. De Gooijer and R. J. Hyndman, 25 Years of Time Series Forecasting, Int. J. Forecast., vol. 22, no. 3, pp. 443–473, 2006.

[73] S. Suhartono, S.P. Rahayu, D. Prastyo, D.G.P. Wijayanti, Juliyanto, Hybrid Model for Forecasting Time Series with Trend, Seasonal and Calendar Variation Patterns, Journal of Physics: Conference Series. 890. 012160. 10.1088/1742-6596/890/1/012160. (2017).

[74] National Renewable Energy Laboratory (NREL), Website: https://maps.nrel.gov/wind-prospector.